

ASYMMETRIC BEAMS IN COSMIC MICROWAVE BACKGROUND ANISOTROPY EXPERIMENTS

J. H. P. Wu¹, A. Balbi^{2,3,4}, J. Borrill^{5,3}, P. G. Ferreira^{6,7}, S. Hanany^{8,3}, A. H. Jaffe^{3,9,1},
A. T. Lee^{10,3,9}, S. Oh^{3,10}, B. Rabbii^{3,10}, P. L. Richards^{10,3}, G. F. Smoot^{10,3,4,9},
R. Stompor^{3,9,11}, C. D. Winant^{3,10}

ABSTRACT

We propose a new formalism to handle asymmetric beams in the data analysis of cosmic microwave background anisotropy experiments. For any beam shape, the formalism finds the optimal circularly symmetric equivalent and is thus easily adaptable to existing data analysis methods. We demonstrate certain key points by using a simulated highly elliptic beam, and the beams and data of the MAXIMA-1 experiment, where the asymmetry is mild. We show that in both cases the formalism does not bias the angular power spectrum estimates. We analyze the limitations of the formalism and find that it is well suited for most practical situations.

Subject headings: cosmic microwave background—cosmology:theory—large-scale structure of the universe—methods:numerical

¹Dept. of Astronomy, University of California, Berkeley, CA, USA

²Dipartimento di Fisica, Università Tor Vergata, Roma, Italy

³Center for Particle Astrophysics, University of California, Berkeley, CA, USA

⁴Lawrence Berkeley National Laboratory, University of California, Berkeley, CA, USA

⁵National Energy Research Scientific Computing Center, Lawrence Berkeley National Laboratory, Berkeley, CA, USA

⁶Astrophysics, University of Oxford, UK

⁷CENTRA, Instituto Superior Tecnico, Lisboa, Portugal

⁸School of Physics and Astronomy, University of Minnesota/Twin Cities, Minneapolis, MN, USA

⁹Space Sciences Laboratory, University of California, Berkeley, CA, USA

¹⁰Dept. of Physics, University of California, Berkeley, CA, USA

¹¹Copernicus Astronomical Center, Warszawa, Poland

1. INTRODUCTION

A new generation of Cosmic Microwave Background (CMB) mapping experiments is beginning to produce data of unprecedented quality (see e.g., Torbet et al. 1999; Miller et al. 1999; DeBernardis et al. 2000; Hanany et al. 2000, hereafter H00). Much of the experimental effort is concentrated on probing angular scales of about 10 arcminutes. To fully benefit from the scientific potential of these high resolution data sets, a new level of sophistication is required in quantifying all possible sources of error in the experimental procedure and data analysis pipeline (e.g., Ferreira & Jaffe 2000). Particular care must be used to accurately quantify the instrument response to the signal and to include such response in the data analysis.

In all analyses of CMB data so far the experimental beam has been assumed to have a radial symmetry. This assumption has been incorporated in most map-making and angular power spectrum (C_ℓ) estimation algorithms (e.g., Bond, Jaffe, & Knox 1998) and is necessary because of limitations in computing capability. A crude symmetric-beam approximation was adequate in the past since most of the error budget was dominated by statistical and other systematic uncertainties. However, with the precision of current and future analyses, it becomes essential to establish a methodology for accurately quantifying the degree of beam-asymmetry and properly incorporating it into the data analysis pipeline. If the beam is incorrectly incorporated in the data analysis pipeline, one may not only artificially distort the underlying structure of the measured CMB signal but also bias the estimate of the CMB angular power spectrum. In this paper we present a new formalism for estimating the power spectrum that can handle any beam shape. We show that the formalism can be applied to a broad variety of cases which encompass most practical applications. As a consequence, the detailed shape of the antenna beam should no longer pose a limitation in measuring the angular power spectrum of CMB experiments.

The asymmetry of beams may arise from a variety of sources. For example, it may be due to the optics, or due to the finite response time of a detector which leaves imprints in the direction of the scan (e.g., Hanany, Jaffe, & Scannapieco 1998). Regardless of the origins of the asymmetry, the framework we shall present is general, and consists of finding an equivalent symmetric beam that replaces the asymmetric beam in the analysis of the data.

Using the formalism one can assess the degree of asymmetry of a beam (see eq. [3-4]), how the asymmetry propagates through the analysis pipeline, and how to find an azimuthally symmetrized beam that best approximates the asymmetric beam (see e.g., eq. [5-9]). The symmetrized beam is then used in the symmetric-beam approximation of the C_ℓ estimation (see eq. [5-11]). The formalism quantifies the errors introduced in the C_ℓ estimates because

of the use of the symmetrized-beam approximation, the uncertainty in the final C_ℓ estimates resulting from the uncertainty in the beam measurement (see eq. [7-5]), and the smoothing effects due to the pixelization of the map (see eqs. [8-8] and [8-9]). It also shows how to combine beams from independent experimental photometers (see eqs. [3-5], [4-10], [4-11], and [4-12]). Some useful conditions under which this new formalism will be needed are also provided (see eqs. [6-5] and [6-7]).

The structure of this paper is as follows. In section 2, we describe the framework of CMB data analysis for the estimation of the power spectrum, so as to illustrate the problems related to asymmetric beams. In section 3, we define the ‘index of asymmetry’ (IOA) ϖ_ℓ , a useful parameter in quantifying the level of asymmetry of a beam. Similarly, we define the ‘index of combined asymmetry’ (IOCA) \mathcal{W}_ℓ , which is useful when combining data from photometers of different beam shapes. In sections 4 and 5, we investigate the problems associated with asymmetric beams. We introduce the ‘average pixel-beam expansion’, $\bar{B}_{p\ell m}$, and the ‘pixel-pixel beam expansion’, $B_{\ell(\text{eff})}^2$, to provide an approximation scheme where the convolution effect of asymmetric beams is treated as circularly symmetric. The biasing effects of this approximation in the resulting estimated power spectrum C_ℓ are also considered. In section 6, we derive the conditions under which one needs to employ the new formalism for treating asymmetric beams. In section 7, we investigate the uncertainties in the C_ℓ estimates resulting from the uncertainties in the measurement of beam shape. In section 8, we discuss another convolution effect due to the pixelization of the CMB map. Although this is not a beam-related issue, we demonstrate a simple way to incorporate its treatment into our framework. In section 9, we numerically verify certain key points developed in sections 3 to 8, as well as the accuracy of the proposed approximation in treating asymmetric beams. In particular, we use the data from the MAXIMA-1 experiment as an example to demonstrate the generic treatment of asymmetric beams in CMB experiments. It is shown that our formalism has no biasing effects in the resulting C_ℓ estimates. Finally in section 10, we summarize the procedure in applying our formalism to experiments, discuss its availability, and draw a conclusion.

2. THE CONVENTION AND PROBLEMS

We first consider the standard procedure for the power spectrum estimation. This consists of two main steps. First, one estimates the pixelized map m_p from a given time-stream d_t , i.e., to translate the observation from the temporal (t) to the spatial (p) domain. Second, one estimates the power spectrum C_ℓ from the map m_p .

In the temporal domain, what we observe is

$$d_t = \gamma_t + n_t, \quad (2-1)$$

where γ_t is the CMB signal and n_t is the instrumental noise. Traditionally we model the CMB observation as

$$\gamma_t = A_{tp} s_p, \quad (2-2)$$

where we use the Einstein summation convention here and below when appropriate (usually over pixels and time samples, but not over spherical harmonic indices). Here A_{tp} is the pointing matrix giving the weight of pixel p in observation t , and s_p is the CMB signal on the pixel convolved by a pixel beam $B_p(\mathbf{x})$:

$$s_p = \sum_{\ell=0}^{\infty} \sum_{m=-\ell}^{\ell} B_{p\ell m} a_{\ell m} Y_{\ell m}(\mathbf{x}_p), \quad (2-3)$$

where $Y_{\ell m}$ are the spherical harmonics, and $B_{p\ell m}$ and $a_{\ell m}$ are the multipole expansions of $B_p(\mathbf{x})$ and the CMB signal respectively. Note that we use a two-dimensional vector \mathbf{x} to denote locations on the surface of the sphere, which we shall often consider in the small-field limit (see later).

We usually take the pointing operator A_{tp} to be one when observing pixel p at time t and zero otherwise. That is, we model the signal γ_t to be the same for any observation within pixel p . In effect, we take the sky to be smoothed with a top-hat of shape given by the pixel boundary. We shall see in section 8 that, as expected, this is equivalent to an extra convolution included in B_p .

With this modeling, one can thus estimate the pixelized map from the temporal data. This involves maximizing the likelihood of the signal given the data:

$$\mathcal{L}(s) \propto \text{Prob}[d|s] = (2\pi)^{-\mathcal{N}_t/2} \times \exp \left\{ -\frac{1}{2} (n^T N^{-1} n + \text{Tr}[\ln N]) \right\}, \quad (2-4)$$

where $d \equiv d_t$, $s \equiv s_p$, and $n \equiv n_t$, all as defined in equations (2-1) and (2-2), \mathcal{N}_t is the size of the time-stream, and $N \equiv N_{tt'} = \langle n_t n_{t'}^T \rangle$ is the time-time noise correlation matrix. Here we have assumed that the noise is Gaussian and that all CMB maps are a priori equally likely. Maximizing over s gives

$$\begin{aligned} m_p \equiv m &= (A^T N^{-1} A)^{-1} (A^T N^{-1} d) \\ &= s_p + n_p, \end{aligned} \quad (2-5)$$

where $A \equiv A_{tp}$ as defined in equation (2-2) and n_p is the noise in the pixel domain.

One then moves on to estimate the power spectrum of the map, $C_\ell = \langle |a_{\ell m}|^2 \rangle$. This requires the maximization of the likelihood function

$$\mathcal{L} = \text{Prob}[m|C_\ell] = (2\pi)^{-\mathcal{N}_{C_\ell}/2} \times \exp \left\{ -\frac{1}{2} (m^T M^{-1} m + \text{Tr}[\ln M]) \right\}, \quad (2-6)$$

where \mathcal{N}_{C_ℓ} is the dimension of the parameter space of C_ℓ , and

$$M \equiv M_{pp'} = C_{Spp'} + C_{Npp'}, \quad (2-7)$$

with

$$C_{Spp'} = \sum_{\ell=0}^{\infty} \sum_{m=-\ell}^{\ell} C_\ell B_{p\ell m} B_{p'\ell m}^* \times Y_{\ell m}(\mathbf{x}_p) Y_{\ell m}^*(\mathbf{x}_{p'}), \quad (2-8)$$

$$C_{Npp'} = (A^T N^{-1} A)^{-1}. \quad (2-9)$$

Here $C_{Spp'} = \langle s_p s_{p'}^T \rangle$ is the pixel-pixel CMB signal correlation matrix, and $C_{Npp'} = \langle n_p n_{p'}^T \rangle$ is the pixel-pixel noise correlation matrix.

We note first that in the estimation of C_ℓ , although there exists methods like the quadratic estimator (Bond et al. 1998) which avoid a direct evaluation of equation (2-6), the relationship between the beam expansion $B_{p\ell m}$ and the power spectrum C_ℓ remains the same and is illustrated in equation (2-8). Second, if the beam is identical for all pixels and circularly symmetric, i.e., $B_{p\ell m} = B_{p'\ell m} = B_\ell$, then equation (2-8) can be greatly simplified as

$$C_{Spp'} = \sum_{\ell=0}^{\infty} \frac{2\ell+1}{4\pi} C_\ell B_\ell^2 P_\ell(\cos \theta_{pp'}), \quad (2-10)$$

where P_ℓ is the Legendre function and $\theta_{pp'} = |\mathbf{x}_p - \mathbf{x}_{p'}|$ is the angular distance between the pixels.

Generally it is impractical to estimate C_ℓ for all ℓ due to the constraints of finite sky coverage and computation power. Instead, one divides the accessible ℓ -range constrained by the sky coverage and the observing beam size into several bands $\{b\}$, and then estimates the band power C_b , i.e., one approximates C_ℓ in the form

$$C_\ell \approx C_b C_\ell^{\text{sh}}, \quad (2-11)$$

where C_ℓ^{sh} is a chosen shape function characterizing the scale dependence in each band. For example, one can choose

$$C_\ell^{\text{sh}} = \frac{1}{\ell(\ell + 1)}, \quad (2-12)$$

which leads to a scale-invariant form in each ℓ band, i.e., $\ell(\ell + 1)C_\ell = \text{const} \quad \forall \ell \in b$. With the approximation (2-11), one can rewrite equation (2-8) as

$$C_{S_{pp'}} \approx \sum_b C_b \mathcal{K}_{pp'b}[C_\ell^{\text{sh}}, B_p, B_{p'}], \quad (2-13)$$

where

$$\begin{aligned} \mathcal{K}_{pp'b}[C_\ell^{\text{sh}}, B_p, B_{p'}] &= \sum_{\ell \in b} \sum_{m=-\ell}^{\ell} C_\ell^{\text{sh}} \times \\ &B_{p\ell m} B_{p'\ell m}^* Y_{\ell m}(\mathbf{x}_p) Y_{\ell m}^*(\mathbf{x}_{p'}). \end{aligned} \quad (2-14)$$

If the beam is symmetric, then one has from equation (2-10) or (2-13) that

$$C_{S_{pp'}} \approx \sum_b C_b \mathcal{K}_b[\theta_{pp'}; C_\ell^{\text{sh}}, B_\ell^2], \quad (2-15)$$

where

$$\begin{aligned} \mathcal{K}_b[\theta_{pp'}; C_\ell^{\text{sh}}, B_\ell^2] &= \\ \sum_{\ell \in b} \frac{2\ell+1}{4\pi} C_\ell^{\text{sh}} B_\ell^2 P_\ell(\cos \theta_{pp'}). \end{aligned} \quad (2-16)$$

In the analysis procedure outlined above, the first problem arises in equations (2-2) and (2-3). Strictly speaking, what is convolved in reality is not the pixel temperature in s_p itself but the CMB signal in the time-stream γ_t , i.e.,

$$\gamma_t = \sum_{\ell=0}^{\infty} \sum_{m=-\ell}^{\ell} B_{t\ell m} a_{\ell m} Y_{\ell m}(\mathbf{x}_t), \quad (2-17)$$

where $B_{t\ell m}$ is the multipole expansion of the time-stream beam $B_t(\mathbf{x})$. This means that the experiment gives us a beam which moves on the sky as a function of time, t , and indeed may observe a different signal within the same pixel, p , depending on the orientation of the beam and the location of its center. We thus make a map which may have many different beams contributing to a single pixel. However, in our analysis formalism we must actually express this map as in (2-3), an observation of the sky with only a single pixel beam, B_p . Hence, for the C_ℓ estimation, we need to find a way to estimate the pixel-beam expansion $B_{p\ell m}$ from the $B_{t\ell m}$, and this will be the focus of sections 4 and 8.

The second problem appears in equation (2-13). If the beam is not symmetric, the summation over m and the dependence on the pixel pair make the exact computation prohibitively expensive. To resolve this problem, in section 5 we introduce the pixel-pixel beam expansion $B_{\ell(\text{eff})}^2$, which provides a consistent way to symmetrize asymmetric beams. This $B_{\ell(\text{eff})}^2$ then replaces the B_{ℓ}^2 in equation (2-15), so as to approximate equation (2-13).

On general grounds, the size of the observing beam is so small that, when necessary, we shall use the flat sky approximation under the small-field limit. This means that when the size of a spherical patch is sufficiently small, the expansion of the beam in spherical harmonics is equivalent to a Fourier transform on a flat two-dimensional patch, i.e.,

$$B_{\ell m} = \int d\Omega B(\mathbf{x}) Y_{\ell m}(\mathbf{x}) \equiv \int dx^2 B(\mathbf{x}) e^{-i\mathbf{k}\cdot\mathbf{x}} = \tilde{B}(\mathbf{k}), \quad (2-18)$$

and

$$\ell \equiv k = |\mathbf{k}|. \quad (2-19)$$

Throughout the paper, we shall use a ‘tilde’ to denote the Fourier transform of a quantity.

3. THE CRITERIA FOR BEAM SYMMETRY

It is important to clearly define the level of asymmetry of an antenna beam. Consider the multipole expansion $B_{\ell m}$ of the beam. For a given ℓ , the variance of $B_{\ell m}$ about its mean over m is

$$\eta_{\ell}^2 = B_{\ell(\text{ms})}^2 - B_{\ell(\text{sm})}^2, \quad (3-1)$$

where $B_{\ell(\text{ms})}^2$ is the mean of squares over m :

$$B_{\ell(\text{ms})}^2 = \langle |B_{\ell m}|^2 \rangle, \quad (3-2)$$

and $B_{\ell(\text{sm})}^2$ is the square of the mean over m :

$$B_{\ell(\text{sm})}^2 = [B_{\ell(\text{m})}]^2 = \langle B_{\ell m} \rangle^2. \quad (3-3)$$

Here $B_{\ell(\text{m})}$ is the mean of $B_{\ell m}$ over m , and therefore can be either positive or negative. We also note that $B_{\ell(\text{ms})}^2$ is the power spectrum of the asymmetric beam, and that $B_{\ell(\text{sm})}^2$ is equivalent to the power spectrum of a symmetric beam that is azimuthally averaged in the real space. Based on this, one can define an ‘index of asymmetry’ (IOA) as

$$\varpi_{\ell} = \frac{\eta_{\ell}}{B_{\ell(\text{ms})}} = \left[1 - \frac{B_{\ell(\text{sm})}^2}{B_{\ell(\text{ms})}^2} \right]^{1/2}. \quad (3-4)$$

We see that ϖ_ℓ varies from zero to one—the larger the ϖ_ℓ , the more asymmetric the beam. We also note that if the beam is symmetric, then ϖ_ℓ is exactly zero. Thus for a given beam, ϖ_ℓ provides us an objective measure of the level of its asymmetry.

In certain situations, we need to combine data from two or more photometers with different beam shapes. We shall use a subscript i ($i = 0, 1, 2$, etc.) to denote the quantities obtained from different photometers. As an analog to equation (3-4), it proves useful to define an ‘index of combined asymmetry’ (IOCA) for all the beams as

$$\mathcal{W}_\ell = \left[1 - \frac{B_{\Sigma\ell(\text{sm})}^2}{B_{\Sigma\ell(\text{ms})}^2} \right]^{1/2}, \quad (3-5)$$

where

$$B_{\Sigma\ell(\text{sm})}^2 = \left[\sum_i \zeta_i B_{i\ell(\text{m})} \right]^2, \quad (3-6)$$

$$B_{\Sigma\ell(\text{ms})}^2 = \left[\sum_i \zeta_i \sqrt{B_{i\ell(\text{ms})}^2} \right]^2, \quad (3-7)$$

the $B_{i\ell(\text{m})}$ and $B_{i\ell(\text{ms})}^2$ are the $B_{\ell(\text{m})}$ and $B_{\ell(\text{ms})}^2$ of photometer i respectively,

$$\zeta_i = \frac{t_{i(\text{obs})}/\text{NET}_i^2}{\sum_i [t_{i(\text{obs})}/\text{NET}_i^2]}, \quad (3-8)$$

$t_{i(\text{obs})}$ is the total observation time of photometer i , and NET_i is its noise equivalent temperature (NET). Here $B_{\Sigma\ell(\text{sm})}^2$ is the square of the noise-weighted mean of B_i , and $B_{\Sigma\ell(\text{ms})}^2$ is the noise-weighted mean of the squares of B_i assuming all the B_i are fully correlated. As one can see, the \mathcal{W}_ℓ varies between zero and one—the larger the \mathcal{W}_ℓ , the more asymmetric a ζ_i -weighted combined beam can be (depending on the detailed orientations of the beams in the temporal samples; we shall discuss this later). This also means that the IOA (ϖ_ℓ) of an average beam with a weight ζ_i for each B_i is always equal to or smaller than \mathcal{W}_ℓ , although the individual $\varpi_{i\ell}$ of B_i may be larger than \mathcal{W}_ℓ . If $\mathcal{W}_\ell = 0$, then we know that all the beams are symmetric ($\varpi_{i\ell} = 0$), and vice versa.

For the purpose of power spectrum estimation, one can employ $\varpi_{i\ell}$ (or \mathcal{W}_ℓ when combining data of different observing beams) to decide if a simple symmetric-beam approximation is sufficient. For example, at ℓ 's where $\varpi_\ell \approx 0$, we expect equation (2-15) to be adequate. On the other hand, at ℓ 's where ϖ_ℓ (or \mathcal{W}_ℓ) deviates significantly from zero, one may need to employ equation (2-13). We shall further discuss these situations, and the use of the IOA (ϖ_ℓ) and the IOCA (\mathcal{W}_ℓ) later.

4. THE AVERAGE PIXEL-BEAM EXPANSION

4.1. The pixel-beam expansion

We first estimate the ‘pixel-beam expansion’, $B_{p\ell m}$, from given observing beams, $B_{t\ell m}$. A naive way to investigate this is to substitute equations (2-3) and (2-17) into the model (2-2), leading to

$$A_{tp}B_{p\ell m}Y_{\ell m}(\mathbf{x}_p) = B_{t\ell m}Y_{\ell m}(\mathbf{x}_t). \quad (4-1)$$

This equation holds if and only if there exists one \mathbf{x}_p for every \mathbf{x}_t such that $\mathbf{x}_t = \mathbf{x}_p$. In this case, we have $B_{p\ell m} = B_{t\ell m}$. This is of course true when the pixel size is infinitesimal, but is unlikely to be fulfilled in reality. Nevertheless, equation (4-1) is just the result of the modeling and therefore not necessarily a requirement in practice. In our formalism for the power spectrum estimation, the s_p is an unknown quantity to be estimated by using equation (2-5), so the actual relation between $B_{p\ell m}$ and $B_{t\ell m}$ should be also obtained through the same process. First, we substitute equation (2-1) into (2-5), and the CMB signal part yields

$$s_p = C_N A^T N^{-1} \gamma_t, \quad (4-2)$$

where $C_N \equiv C_{N_{pp'}}$ as defined in equation (2-9). Further substituting equations (2-3) and (2-17) into this result, we obtain

$$B_{p\ell m}Y_{\ell m}(\mathbf{x}_p) = C_N A^T N^{-1} B_{t\ell m}Y_{\ell m}(\mathbf{x}_t). \quad (4-3)$$

This equation is completely general, and should be in principle satisfied when one tries to find the $B_{p\ell m}$ from the given $B_{t\ell m}$. We thus see that equation (4-1) is just one of the solutions to equation (4-3), but not necessarily a requirement for the purpose of power spectrum estimation.

In most cases, the noise n_t in each temporal measure is nearly independent from the others, so the time-time noise correlation matrix $N_{tt'}$ is diagonal, with the tt elements equal to the noise variance at each time sample, i.e.,

$$N_{tt'} = \mu_t^2 \delta(t - t'), \quad (4-4)$$

where μ_t is the standard deviation of time sample t , and $\delta(t - t')$ is a Dirac Delta. This allows us to simplify equation (4-3) as

$$B_{p\ell m}Y_{\ell m}(\mathbf{x}_p) = \sum_{t \in p} \xi_t B_{t\ell m}Y_{\ell m}(\mathbf{x}_t), \quad (4-5)$$

where ξ_t is the noise-estimated statistical weight at t :

$$\xi_t = \frac{\mu_t^{-2}}{\sum_{t \in p} \mu_t^{-2}}. \quad (4-6)$$

For simplicity, we shall take this white-noise assumption for further investigation. We consider the more general case of correlated noise in the Appendix, and show that this white-noise approximation is appropriate in most practical cases. The conditions for the use of this white-noise assumption will be also derived in the Appendix (see eq. [A10]).

To further simplify equation (4-5), we assume that $\mathbf{x}_t \equiv \mathbf{x}_p \forall t \in p$ (i.e., the temporal measure γ_t is thought of as a ‘sample’ of the pixel temperature s_p ; see eq. [4-2]), so that the pixel-beam expansion can now be obtained as

$$B_{p\ell m} = \sum_{t \in p} \xi_t B_{t\ell m}. \quad (4-7)$$

The assumption, $\mathbf{x}_t \equiv \mathbf{x}_p$, for achieving this result will be relaxed in section 8, where we show that only an extra correction is required.

4.2. The average pixel-beam expansion

As will be shown, it proves useful to remove the pixel dependence of $B_{p\ell m}$ in the formalism of the C_ℓ estimation. We thus consider the noise-weighted average of $B_{p\ell m}$ over all pixels (c.f. eq. [2-5]):

$$\overline{B}_{p\ell m} = H(U^T C_N^{-1} B_{p\ell m}), \quad (4-8)$$

where $U \equiv U_p$ is a contraction vector with entries all equal to unity, and

$$H = (U^T C_N^{-1} U)^{-1}. \quad (4-9)$$

We shall call $\overline{B}_{p\ell m}$ the ‘average pixel-beam expansion’. We note that the subscript p in $\overline{B}_{p\ell m}$ does not mean the pixel dependence as in the usual convention, but indicates that this is a mean taken over all pixels.

With the white-noise assumption (eq. [4-4]), the $\overline{B}_{p\ell m}$ can be calculated explicitly by substituting equation (4-7) into equation (4-8):

$$\overline{B}_{p\ell m} = \sum_t \chi_t B_{t\ell m}, \quad (4-10)$$

where

$$\chi_t = \frac{\mu_t^{-2}}{\sum_t \mu_t^{-2}}. \quad (4-11)$$

If the data are from a single photometer with a constant noise level, then equation (4-10) reduces to a simple linear average of all time-stream beams. If the data are combined from

different photometers, then the μ_t can be approximated as (c.f. eq. [3-8])

$$\mu_t = \frac{\text{NET}_t}{\sqrt{\delta t_{(\text{obs})}}}, \quad (4-12)$$

where NET_t is the NET of the corresponding photometer at time t , and $\delta t_{(\text{obs})}$ is the integration time of the temporal observation at t . If the integration time remains unchanged among photometers, then the μ_t in equation (4-11) can be simply taken as the NET of the corresponding photometer. We also note that with the definition (4-12), equations (3-8) and (4-11) can be related as

$$\zeta_i = \sum_{t \in i} \chi_t, \quad (4-13)$$

meaning that ζ_i is the total noise-estimated weight of photometer i .

We note that in cases where both the shape of the experimental beam and its orientation relative to the pixel are roughly constant throughout the observation, we have a reasonable approximation (see eq. [4-10]):

$$\overline{B}_{p\ell m} \approx B_{t\ell m}. \quad (4-14)$$

In other cases, equation (4-10) will need to be employed, for example, when the relative orientation between the asymmetric beam and the pixels changes, or when data from different photometers are combined together. We also note that even if all the beams B_i of different photometers are symmetric (i.e., $\varpi_{i\ell} = \mathcal{W}_\ell = 0$), the $B_{p\ell m}$ may still have pixel dependence due to the various relative contribution of B_i within different pixels (see eq. [4-7]). In such cases, one will need to consider equation (4-10), and a simple formalism like equation (2-15) will be invalid for the estimation of the CMB angular power spectrum, since the $B_{p\ell}^2$ is different on each pixel. As will be shown, the formalism we shall develop is also capable of dealing with this situation.

4.3. Useful Limits

We now derive useful constraints on the magnitude of the average pixel-beam expansion $\overline{B}_{p\ell m}$. In the small-field limit, the power spectrum of $\overline{B}_{p\ell m}$ can be written as (see eqs. [2-18], [3-2], and [4-10])

$$\overline{B}_{p\ell(\text{ms})}^2 \equiv \frac{1}{\pi} \int_0^\pi d\varphi \left| \sum_t \chi_t \tilde{B}_t(\mathbf{k}) \right|^2, \quad (4-15)$$

where φ is the phase angle of \mathbf{k} on the ring $|\mathbf{k}| = k$. We first consider single-photometer experiments. In this case, if the beam pattern remains the same throughout the entire

observation but with only different orientations at different t , then we can rewrite B_t as

$$B_t = A(\beta_t)B_0, \quad (4-16)$$

where $A(\beta_t)$ is the rotation matrix, β_t is the rotation angle at time t with respect to $t = 0$, and B_0 is the shape of the time-stream beam at $t = 0$. Substituting this into equation (4-15) gives

$$\overline{B}_{p\ell(\text{ms})}^2 \equiv \frac{1}{\pi} \int_0^\pi d\varphi \left| \int_0^{2\pi} f(\beta) A(\beta) \tilde{B}_0(\mathbf{k}) d\beta \right|^2, \quad (4-17)$$

where $f(\beta)$ is the weighting function of a rotation angle β , and satisfies $\int_0^{2\pi} d\beta f(\beta) = 1$. It is then straightforward to show that the function $f(\beta)$ that minimizes the right hand side of the above equation is $f(\beta) = 1/2\pi$, leading to

$$\overline{B}_{p\ell(\text{ms})}^2 \Big|_{\min} \equiv \left[\frac{1}{\pi} \int_0^\pi d\varphi \tilde{B}_0(\mathbf{k}) \right]^2 \equiv B_{0\ell(\text{sm})}^2, \quad (4-18)$$

where $B_{0\ell(\text{sm})}^2$ is as defined in equation (3-3). On the other hand, the function $f(\beta)$ that maximizes the right hand side of equation (4-17) is $f(\beta) = \delta(\beta - \beta_0)$ (Dirac Delta, $\beta_0 \in \{0, 2\pi\}$), and this gives

$$\overline{B}_{p\ell(\text{ms})}^2 \Big|_{\max} \equiv \frac{1}{\pi} \int_0^\pi d\varphi \left| \tilde{B}_0(\mathbf{k}) \right|^2 \equiv B_{0\ell(\text{ms})}^2, \quad (4-19)$$

where $B_{0\ell(\text{ms})}^2$ is as defined in equation (3-2). These results tell us that when the pixels are scanned almost uniformly in all directions, then the resulting $\overline{B}_{p\ell(\text{ms})}^2$ should be closer to $\overline{B}_{p\ell(\text{ms})}^2 \Big|_{\min} = B_{0\ell(\text{sm})}^2$. When the pixels are scanned with an almost fixed direction, then the resulting $\overline{B}_{p\ell(\text{ms})}^2$ should be closer to $\overline{B}_{p\ell(\text{ms})}^2 \Big|_{\max} = B_{0\ell(\text{ms})}^2$. Thus, we have a good check of the numerically calculated $\overline{B}_{p\ell m}$ from equation (4-10) (or eq. [4-17]), i.e., a constraint on the amplitude of $\overline{B}_{p\ell(\text{ms})}^2$:

$$B_{0\ell(\text{ms})}^2 \geq \overline{B}_{p\ell(\text{ms})}^2 \geq B_{0\ell(\text{sm})}^2, \quad (4-20)$$

or equivalently,

$$1 \geq \frac{\overline{B}_{p\ell(\text{ms})}^2}{B_{0\ell(\text{ms})}^2} \geq 1 - \varpi_{0\ell}^2, \quad (4-21)$$

where $\varpi_{0\ell}$ is the IOA of B_0 . For symmetric beams, all the equality signs hold. In experiments, one can take B_0 as the measured beam, and then use equation (3-4) to calculate $\varpi_{0\ell}$.

When we combine data from two or more photometers with different beam shapes, following the same line of development as above gives (see eqs. [3-6], [3-7], [4-10], and [4-13])

$$B_{\Sigma\ell(\text{ms})}^2 \geq \overline{B}_{p\ell(\text{ms})}^2 \geq B_{\Sigma\ell(\text{sm})}^2, \quad (4-22)$$

or equivalently,

$$1 \geq \frac{\overline{B}_{p\ell(\text{ms})}^2}{B_{\Sigma\ell(\text{ms})}^2} \geq 1 - \mathcal{W}_\ell^2, \quad (4-23)$$

where \mathcal{W}_ℓ is the IOCA defined in equation (3-5). We shall further discuss the use of these limits later.

5. THE PIXEL-PIXEL BEAM EXPANSION

5.1. Formalism

In the data analysis procedure briefly demonstrated in section 2, the effect of asymmetric beam convolution manifests itself in equation (2-8). However, the summation over m and the dependence on the pixel pair make it computationally expensive. Therefore, we prefer to use the form of equation (2-10) as an approximation. This can be achieved by replacing the B_ℓ^2 in equation (2-10) with a ‘pixel-pixel beam expansion’ $B_{\ell(\text{eff})}^2$, which we shall derive in this section.

First, one can replace the B_ℓ^2 in equation (2-10) with

$$B_{pp'\ell}^2 = \frac{4\pi \sum_m B_{p\ell m} B_{p'\ell m}^* Y_{\ell m}(\mathbf{x}_p) Y_{\ell m}^*(\mathbf{x}_{p'})}{(2\ell + 1) P_\ell(\cos \theta_{pp'})}, \quad (5-1)$$

so that equation (2-10) is equivalent to equation (2-8). In the small-field limit, equation (5-1) becomes

$$B_{pp'\ell}^2 \equiv B_{pp'k}^2 = \frac{\mathcal{J} [k\Delta x, \varphi_0; \tilde{\mathcal{B}}_{pp'}^2(\mathbf{k})]}{J_0(k\Delta x)}, \quad (5-2)$$

where

$$\begin{aligned} \mathcal{J} [k\Delta x, \varphi_0; \tilde{\mathcal{B}}_{pp'}^2(\mathbf{k})] = \\ \frac{1}{\pi} \int_0^\pi d\varphi \left\{ \Re [\tilde{\mathcal{B}}_{pp'}^2(\mathbf{k})] \cos[k\Delta x \cos(\varphi - \varphi_0)] \right. \\ \left. - \Im [\tilde{\mathcal{B}}_{pp'}^2(\mathbf{k})] \sin[k\Delta x \cos(\varphi - \varphi_0)] \right\}, \end{aligned} \quad (5-3)$$

$\Delta \mathbf{x} = \mathbf{x}_p - \mathbf{x}_{p'}$, $\Delta x = |\Delta \mathbf{x}| \equiv \theta_{pp'}$, φ_0 is the phase angle of $\Delta \mathbf{x}$, J_0 is the Bessel function of the first kind of integral order 0, $\tilde{\mathcal{B}}_{pp'}^2(\mathbf{k}) = \tilde{B}_p(\mathbf{k}) \tilde{B}_{p'}^*(\mathbf{k})$, and \Re and \Im indicate the real and imaginary parts of $\tilde{\mathcal{B}}_{pp'}^2$, respectively. We notice that $\mathcal{J}[k\Delta x, \varphi_0; 1] = J_0(k\Delta x)$. Therefore if the beam is circularly symmetric and remains the same on all pixels, i.e., $\tilde{\mathcal{B}}_{pp'}^2(\mathbf{k}) \equiv \tilde{B}_k^2$, then

$\mathcal{J}[k\Delta x, \varphi_0; \widetilde{\mathcal{B}}_{pp'}^2(\mathbf{k})] = \mathcal{J}[k\Delta x, \varphi_0; \widetilde{B}_k^2] = J_0(k\Delta x)\widetilde{B}_k^2$, so that $B_{pp'k}^2$ in equation (5-2) becomes \widetilde{B}_k^2 exactly as required.

To save computation time and memory when estimating C_l , we need to remove the dependence of $B_{pp'\ell}^2$ on the particular choice of a pixel pair $(\mathbf{x}_p, \mathbf{x}_{p'})$. We achieve this by taking the average of $B_{pp'\ell}^2$ over all possible $(\mathbf{x}_p, \mathbf{x}_{p'})$ pairs:

$$B_{\ell(\text{eff})}^2 = \langle B_{pp'\ell}^2 \rangle. \quad (5-4)$$

We call this $B_{\ell(\text{eff})}^2$ the ‘pixel-pixel beam expansion’.

Even with this, equation (5-4) together with equation (5-2) is still computationally expensive and may not be feasible. Therefore we further simplify the formalism in the following way. First, we remove the dependence of $\widetilde{\mathcal{B}}_{pp'}^2(\mathbf{k})$ in equation (5-2) on pixel pairs, by replacing it with a noise-weighted average (c.f. eqs. [2-5] and [4-8])

$$\overline{\widetilde{\mathcal{B}}_{pp'}^2} = (U^T C_N^{-1} U U^T C_N^{-1} U)^{-1} (U^T C_N^{-1} \widetilde{\mathcal{B}}_{pp'}^2 C_N^{-1} U). \quad (5-5)$$

Here the subscript pp' in $\overline{\widetilde{\mathcal{B}}_{pp'}^2}$ does not mean the pixel pair dependence as in the usual convention, but indicates that the mean is taken over all pixel pairs. With this replacement, equation (5-2) is now only a function of $\Delta\mathbf{x}$ for a given $\ell \equiv k$. Thus when evaluating equation (5-4), we can classify all possible $\Delta\mathbf{x}$ into several groups of different Δx , each with several subgroups of different φ_0 . This gives

$$B_{\ell(\text{eff})}^2 \equiv \sum_{\Delta x, \varphi_0} g(\Delta x, \varphi_0) \frac{\mathcal{J} \left[k\Delta x, \varphi_0; \overline{\widetilde{\mathcal{B}}_{pp'}^2}(\mathbf{k}) \right]}{J_0(k\Delta x)}, \quad (5-6)$$

where $g(\Delta x, \varphi_0)$ is the weight of the configuration $(\Delta x, \varphi_0)$, i.e., the number of pixel pairs with Δx and φ_0 , divided by the total number of pixel pairs. It satisfies $\sum_{\Delta x, \varphi_0} g(\Delta x, \varphi_0) = 1$. This algorithm can normally reduce the number of operations in equation (5-4) by several orders of magnitude, because the element number of $\{(\Delta x, \varphi_0)\}$ is normally several orders below that of $\{(\mathbf{x}_p, \mathbf{x}_{p'})\}$. In addition, if the number of pixels is large enough as in most cases, then φ_0 is nearly uniformly distributed between 0 and 2π for every given Δx , depending on the relative locations of all pixels. In this case, after the summation over φ_0 at each given Δx in equation (5-6), the first term inside the integral in equation (5-3) (which enters eq. [5-6]) becomes $\Re \left[\overline{\widetilde{\mathcal{B}}_{pp'}^2}(\mathbf{k}) \right] J_0(k\Delta x)$ and the second term vanishes. Thus the Bessel function in equation (5-6) can be removed and we have

$$B_{\ell(\text{eff})}^2 \approx \frac{1}{\pi} \int_0^\pi \Re \left[\overline{\widetilde{\mathcal{B}}_{pp'}^2}(\mathbf{k}) \right] d\varphi. \quad (5-7)$$

With careful simplification of the real part of equation (5-5), we also find that

$$\Re \left[\overline{\mathcal{B}_{pp'}^2(\mathbf{k})} \right] = \left| \overline{B_p(\mathbf{k})} \right|^2, \quad (5-8)$$

where $\overline{B_p(\mathbf{k})} \equiv \overline{B_{p\ell m}}$ as defined in equation (4-8). We note that the average over all pixel pairs (the left-hand side of eq. [5-8]) is now reduced to the average over all pixels (the right-hand side). This further enables us to simplify equation (5-7) as

$$B_{\ell(\text{eff})}^2 \approx \frac{1}{\pi} \int_0^\pi \left| \overline{B_p(\mathbf{k})} \right|^2 d\varphi \equiv \overline{B_{p\ell(\text{ms})}^2}, \quad (5-9)$$

where the last step uses the definition (3-2), and the $\overline{B_{p\ell(\text{ms})}^2}$ is readily evaluated in equation (4-15). When calculating $\overline{B_{p\ell(\text{ms})}^2}$, one can take the form of equation (4-17) to save computation time. We note that the approximation sign above will become equality when φ_0 is uniformly distributed between 0 and 2π . In section 9, we shall numerically verify this result.

With such, now we can use the form of equation (2-10) to approximate equation (2-8) in the presence of asymmetric beams or when combining data with different symmetric beams. In other words, we have equation (2-8) being approximated as

$$C_{Spp'} \approx \sum_{\ell=0}^{\infty} \frac{2\ell+1}{4\pi} C_\ell B_{\ell(\text{eff})}^2 P_\ell(\cos \theta_{pp'}). \quad (5-10)$$

Furthermore, as illustrated in equations (2-11) through (2-16) and the context, one normally divides the ℓ range under investigation into several bands, due to the finite sizes of the sky coverage and the observing beam, as well as the limited computation power. Using this formalism, we can approximate equation (2-13) using equation (2-15) with its B_ℓ^2 replaced by the $B_{\ell(\text{eff})}^2$ calculated above. This gives

$$C_{Spp'} \approx \sum_b C_b \mathcal{K}_b[\theta_{pp'}; C_\ell^{\text{sh}}, B_{\ell(\text{eff})}^2]. \quad (5-11)$$

5.2. Uncertainties

When making the approximation (5-10), we inevitably induce errors in the basis $B_{\ell(\text{eff})}^2 P_\ell(\cos \theta_{pp'})$ for each pixel pair. These errors can be represented as

$$\frac{B_{pp'\ell}^2}{B_{\ell(\text{eff})}^2} \equiv 1 \pm \sigma_\ell, \quad (5-12)$$

where σ_ℓ is the normalized standard deviation of the errors. This deviation can be simultaneously evaluated while one performs equation (5-6), i.e.,

$$\sigma_\ell^2 = \sum_{\Delta x, \varphi_0} g(\Delta x, \varphi_0) \left\{ \frac{\mathcal{J} \left[k\Delta x, \varphi_0; \widetilde{\mathcal{B}}_{pp'}^2 \right]}{B_{\ell(\text{eff})}^2 J_0(k\Delta x)} \right\}^2 - 1. \quad (5-13)$$

Since C_ℓ appears in combination with $B_{\ell(\text{eff})}^2 P_\ell(\cos \theta_{pp'})$ (see eq. [5-10]), we know that σ_ℓ basically quantifies the bias in C_ℓ for each individual pixel pair. Nevertheless, the resulting bias in the final C_ℓ estimates by using the approximation (5-10) together with the likelihood analysis (see eq. [2-6] and context) may be much smaller than σ_ℓ , because the resulting C_ℓ is a consequence of the contribution from *all* pixel pairs. For example, if all pixel pairs contribute to the likelihood function (2-6) as a linear combination of $B_{pp'\ell}^2 P_\ell(\cos \theta_{pp'})$, then the resulting bias in C_ℓ will be as small as $\sigma_\ell/\mathcal{N}_p$, where \mathcal{N}_p is the total number of pixels. Although we know that reality is not like such a simple case, we can still quantify the bias of approximation (5-10) using numerical simulations.

Similarly, we can consider the errors in the band power C_b for each individual pixel pair, resulting from the approximation (5-11). Since C_b is coupled with \mathcal{K}_b (eq. [5-11]) or $\mathcal{K}_{pp'b}$ (eq. [2-13]), the errors in C_b for each individual pixel pair may be quantified by comparing \mathcal{K}_b and $\mathcal{K}_{pp'b}$, as we did for $B_{\ell(\text{eff})}^2$ and $B_{pp'\ell}^2$. However, as argued earlier, the result calculated in this way quantifies only the errors in C_b for each individual pixel pair, and the real bias of the approximation (5-11) together with the likelihood analysis may be much smaller. We shall quantify the real systematic bias of this approximation in section 9, using numerical simulations.

6. SYMMETRY VS. ASYMMETRY

In this section, we investigate the conditions under which one needs to employ the formalism for treating asymmetric beams, i.e. the formalism we developed in the previous two sections. We first consider the case where the data to be analyzed is from only one photometer. From equation (5-9), we know that the pixel-pixel beam expansion $B_{\ell(\text{eff})}^2$ can be approximated by $\overline{B}_{p\ell(\text{ms})}^2$, and therefore should be also constrained by equation (4-21), resulting in

$$1 \geq \frac{B_{\ell(\text{eff})}^2}{B_{0\ell(\text{ms})}^2} \geq 1 - \varpi_{0\ell}^2. \quad (6-1)$$

This implies that if we simply use $B_{0\ell(\text{ms})}^2$ (where B_0 is the measured beam shape from the experiment) as the $B_{\ell(\text{eff})}^2$ in our formalism, then $B_{\ell(\text{eff})}^2$ will be overestimated by at most $\varpi_{0\ell}^2/(1 - \varpi_{0\ell}^2)$.

Furthermore, we consider the errors in C_ℓ resulting from this effect. In our formalism, the beam convolution appears as the multiplication of $B_{\ell(\text{eff})}^2$ and C_ℓ (see eq. [5-10]), so the errors in C_ℓ can be expressed as

$$\delta_{C_\ell} = \frac{dC_\ell}{C_\ell} = \frac{dB_{\ell(\text{eff})}^{-2}}{B_{\ell(\text{eff})}^{-2}}. \quad (6-2)$$

Taking $dB_{\ell(\text{eff})}^{-2} = B_{0\ell(\text{ms})}^{-2} - B_{\ell(\text{eff})}^{-2}$, we have from equations (6-1) and (6-2) that

$$0 \geq \delta_{C_\ell} \geq -\varpi_{0\ell}^2. \quad (6-3)$$

This means that when we use $B_{0\ell(\text{ms})}^2$ as the $B_{\ell(\text{eff})}^2$ in our formalism, then the resulting C_ℓ at a given ℓ will be *underestimated* by at most $\varpi_{0\ell}^2$. To share this error on both sides of a mis-estimated C_ℓ , we can choose the $B_{\ell(\text{eff})}^2$ to be

$$B_{0\ell(\text{mid})}^2 = \frac{2}{B_{0\ell(\text{ms})}^{-2} + B_{0\ell(\text{sm})}^{-2}} = \frac{1 - \varpi_{0\ell}^2}{1 - \varpi_{0\ell}^2/2} B_{0\ell(\text{ms})}^2, \quad (6-4)$$

so that the resulting error in the C_ℓ estimates is now constrained as

$$\frac{\varpi_{0\ell}^2}{2 - 2\varpi_{0\ell}^2} \geq \delta_{C_\ell(\text{mid})} \geq -\frac{\varpi_{0\ell}^2}{2}. \quad (6-5)$$

When $\varpi_{0\ell}^2 \ll 1$, we have $|\delta_{C_\ell(\text{mid})}| \lesssim \varpi_{0\ell}^2/2$. If the beam is symmetric, then all the equality signs above hold and $B_{0\ell(\text{ms})}^2 = B_{0\ell(\text{mid})}^2 = B_{0\ell(\text{sm})}^2 = B_{\ell(\text{eff})}^2$.

Following the same line of logic, we now consider the cases where the data to be analyzed is combined from two or more photometers. In this case, it is also straightforward to show that if we choose the $B_{\ell(\text{eff})}^2$ to be (see also eqs. [3-6] and [3-7] for definitions)

$$B_{\Sigma\ell(\text{mid})}^2 = \frac{2}{B_{\Sigma\ell(\text{ms})}^{-2} + B_{\Sigma\ell(\text{sm})}^{-2}} = \frac{1 - \mathcal{W}_\ell^2}{1 - \mathcal{W}_\ell^2/2} B_{\Sigma\ell(\text{ms})}^2, \quad (6-6)$$

then the errors in the C_ℓ estimates are constrained as

$$\frac{\mathcal{W}_\ell^2}{2 - 2\mathcal{W}_\ell^2} \geq \delta_{C_\ell(\text{mid})} \geq -\frac{\mathcal{W}_\ell^2}{2}. \quad (6-7)$$

When $\mathcal{W}_\ell^2 \ll 1$, we have $|\delta_{C_\ell(\text{mid})}| \lesssim \mathcal{W}_\ell^2/2$. If all the beams are symmetric ($\varpi_{i\ell} = 0$), then all the equality signs above hold.

As a result, we see that if the $\varpi_{0\ell}^2/2$ (or $\mathcal{W}_\ell^2/2$) is well below the tolerated maximum error of C_ℓ , then we can use $B_{0\ell(\text{mid})}^2$ (or $B_{\Sigma\ell(\text{mid})}^2$) as the $B_{\ell(\text{eff})}^2$ in the symmetric-beam formalism, i.e., we can simply use equation (2-15) with $B_\ell^2 = B_{0\ell(\text{mid})}^2$ (or $B_{\Sigma\ell(\text{mid})}^2$), without the need of going through the procedure developed in sections 4 and 5. The associated errors in the final C_ℓ estimates will be constrained by equation (6-5) (or eq. [6-7]).

7. UNCERTAINTIES FROM BEAM MEASUREMENT

It is inevitable for any experiment that there are uncertainties in the measurement of the beam shapes. It is therefore crucial to quantify the uncertainties in the final C_ℓ estimates resulting from this beam shape uncertainties. For a given beam $B(\mathbf{x})$, consider an uncertainty ϵ in the full width at half maxima (FWHM), and assume that the uncertainties at all iso-height contours of the beam are a fixed fraction of the contour sizes, i.e.,

$$\frac{d\mathbf{x}}{\mathbf{x}} = \epsilon. \quad (7-1)$$

This uncertainty in the beam shape will then be transferred to the multipole space as the uncertainty in ℓ at a given height $B_{\ell m}$:

$$\frac{d\ell}{\ell} = -\epsilon. \quad (7-2)$$

This results in the uncertainty in B_ℓ^2 at a given ℓ

$$\Delta_{B_\ell^2} = \frac{dB_\ell^2}{B_\ell^2} = \frac{B_{(1+\epsilon)\ell}^2}{B_\ell^2} - 1. \quad (7-3)$$

We then consider the change in the C_ℓ estimates:

$$\Delta_{C_\ell} = \frac{dC_\ell}{C_\ell}. \quad (7-4)$$

Since the beam convolution occurs as the multiplication of B_ℓ^2 and C_ℓ (see eqs. [2-8] and [5-10]; here we have dropped the subscript ‘(eff)’ for concise notation), we know that the resulting uncertainty in C_ℓ is

$$\Delta_{C_\ell} = \Delta_{B_\ell^2} = \frac{B_{(1+\epsilon)\ell}^2}{B_\ell^2} - 1. \quad (7-5)$$

This means that if the beam size is mis-estimated by ϵ (i.e., the actual size is $1 + \epsilon$ times the measured size), then the resulting C_ℓ estimates will be $1 + \Delta_{C_\ell}$ times the real C_ℓ . Thus for a given uncertainty in the beam measurement ϵ , one can employ equation (7-5) to estimate the resulting uncertainty in the final C_ℓ estimates. We also note that the banding of ℓ does not affect this result, as we shall show in section 9.3.

We note from the above result that the type of uncertainty we assumed in the measurement of the beam size (eq. [7-1]) induces an error that is correlated between the C_ℓ estimates in all ℓ bins, although the magnitude of the error depends on ℓ . If the power of the beam B_ℓ^2 monotonically decreases with ℓ , a measured beam size slightly larger than the real value

will produce larger C_ℓ estimates at all ℓ bins. Although this is not the most general kind of beam size error, it is quite common.

We now investigate certain special cases. In situations where $\partial B_\ell^2/\partial\ell$ is not changing much within $d\ell$, i.e.,

$$\frac{\partial B_\ell^2}{\partial\ell} \approx \frac{\partial B_{(1+\epsilon)\ell}^2}{\partial\ell}, \quad (7-6)$$

we can approximate equation (7-3) and thus (7-5) as

$$\Delta_{C_\ell} = \Delta_{B_\ell^2} \approx -\frac{d\ell}{B_\ell^2} \frac{\partial B_\ell^2}{\partial\ell} = \frac{2\epsilon\ell}{B_\ell} \frac{\partial B_\ell}{\partial\ell}, \quad (7-7)$$

where equation (7-2) has been employed. For a symmetric Gaussian beam $B(\mathbf{x}) = \exp(-x^2/2\varrho^2)$, equation (7-7) becomes

$$\Delta_{C_\ell(\text{G})} \approx \Delta_{C_\ell(\text{G})}^* = -2\epsilon\varrho^2\ell^2, \quad (7-8)$$

while the condition (7-6), for $|\epsilon| \ll 1$, leads straightforwardly to

$$\ell \ll \ell_{(\text{G})}^* = \frac{1}{\sqrt{2|\epsilon|}\varrho}. \quad (7-9)$$

Here we have again used the small-field limit. When combined with the condition (7-9), we find that approximation (7-8) breaks down when $|\Delta_{C_\ell(\text{G})}^*|$ is comparable with unity. In particular, we investigate the accuracy of approximation (7-8), by comparing it with equation (7-5). We find for $|\epsilon| < 20\%$ that the approximation is accurate within 10% error if

$$\ell < \ell_{(\text{G};10\%)}^* = (0.44 + 0.8|\epsilon|) \ell_{(\text{G})}^*, \quad (7-10)$$

where $\ell_{(\text{G})}^*$ is given in equation (7-9). For example, if $\epsilon = 10\%$ and the Gaussian beam has a FWHM of 10 arcminutes (i.e., $\varrho = 1.24 \times 10^{-3}$ radians), then approximation (7-8) is accurate within 10% error when $\ell < \ell_{(\text{G};10\%)}^* \approx 940$. Under the condition (7-10), one can see from equation (7-8) that, for an approximately Gaussian beam, the resulting uncertainty in the final C_ℓ estimates increases in proportion to the uncertainty in the beam measurement ϵ , the square of the beam size ϱ^2 , and the square of the multipole number ℓ^2 .

8. DECONVOLUTION OF THE PIXEL SMOOTHING

We have not dealt with the smoothing effects due to the pixelization of the map, when translating the data from the temporal to the pixel domain (see eqs. [2-5] and [4-3]). Because convolving a CMB map with a Dirac Delta $\delta(\mathbf{x} - \mathbf{x}_1)$ will shift the original temperature at

\mathbf{x} to a new location $\mathbf{x} + \mathbf{x}_1$, we know that $Y_{\ell m}(\mathbf{x}) = \delta_{\ell m}(\mathbf{x}_1)Y_{\ell m}(\mathbf{x} + \mathbf{x}_1)$ where $\delta_{\ell m}(\mathbf{x}_1)$ is the multipole expansion of $\delta(\mathbf{x} - \mathbf{x}_1)$. This allows us to rewrite equation (4-3) as

$$B_{p\ell m} = C_N A^T N^{-1} B_{t\ell m} \delta_{\ell m}(\mathbf{x}_p - \mathbf{x}_t). \quad (8-1)$$

Substituting this into equation (4-8), we obtain

$$\bar{B}_{p\ell m} = H U^T C_N^{-1} \text{diag}(C_N A^T N^{-1} B_{\delta\ell m}), \quad (8-2)$$

where $B_{\delta\ell m} \equiv B_{t\ell m} \delta_{\ell m}(\mathbf{x}_p - \mathbf{x}_t)$ is a \mathcal{N}_t by \mathcal{N}_p matrix, and $\text{diag}(M)$ is a vector whose entries are the diagonal elements of the matrix M . These results are completely general. Without further information about N^{-1} or $B_{\delta\ell m}$, equation (8-2) can not be simplified, mainly due to the involvement of $\delta_{\ell m}(\mathbf{x}_p - \mathbf{x}_t)$.

With the white-noise assumption (see sec. 4.1), we have equation (8-1) simplified as

$$B_{\Pi p\ell m} = \sum_{t \in p} \xi_t B_{t\ell m} \delta_{\ell m}(\mathbf{x}_p - \mathbf{x}_t), \quad (8-3)$$

and equation (8-2) as

$$\bar{B}_{\Pi p\ell m} = \sum_t \chi_t B_{t\ell m} \delta_{\ell m}(\mathbf{x}_{p \ni t} - \mathbf{x}_t), \quad (8-4)$$

where $\mathbf{x}_{p \ni t}$ is the central coordinates of the pixel p that covers \mathbf{x}_t , and ξ_t and χ_t are as defined in equations (4-6) and (4-11) respectively. Here we use the subscript ‘ Π ’ to distinguish these results from those in equations (4-7) and (4-10). In the real space, equation (8-4) is equivalent to

$$\bar{B}_{\Pi p}(\mathbf{x}) = \sum_t \chi_t B_t(\mathbf{x} - \mathbf{x}_{p \ni t} + \mathbf{x}_t), \quad (8-5)$$

meaning that $\bar{B}_{\Pi p}$ is the noise-weighted average over the time-stream beams B_t that are shifted by $\mathbf{x}_{p \ni t} - \mathbf{x}_t$ at each time t . This implies that our formalism developed previously is still available, requiring only a modification that takes into account the detailed locations of the temporal hits \mathbf{x}_t with respect to the pixel centers $\mathbf{x}_{p \ni t}$. Thus we have relaxed the assumption $\mathbf{x}_t \equiv \mathbf{x}_{p \ni t}$ that was made to achieve equations (4-7) and (4-10).

In most cases, both \mathcal{N}_p and \mathcal{N}_t are large, and the beam shape B_t of each photometer does not change much within several successive pixels. This results in the fact that in determining the $\bar{B}_{\Pi p}$ in equation (8-5), each beam configuration $A(\beta)B_0(\mathbf{x})$ (see eq. [4-16]) appears at a set of \mathbf{x}_t which have offsets $\mathbf{x}_{p \ni t} - \mathbf{x}_t$ distributed within a region that is confined by the pixel shapes. If all pixels have the same shape, then this is equivalent to convolving each $A(\beta)B_0(\mathbf{x})$ with a top-hat like window whose boundary is defined by the pixel shape. As a result, we can approximate equation (8-4) as

$$\bar{B}_{\Pi p\ell m} \approx \bar{B}_{p\ell m} \Pi_{\ell m}, \quad (8-6)$$

where $\overline{B}_{p\ell m}$ is as defined in equation (4-10), and $\Pi_{\ell m}$ is the multipole expansion of

$$\Pi(\mathbf{x}) = \sum_t \delta(\mathbf{x}_{p\supset t} - \mathbf{x}_t). \quad (8-7)$$

The same also applies to the simple case where all time-stream beams B_t are the same. We thus see that the $\Pi_{\ell m}$ in equation (8-6) serves as an extra convolution (apart from the time-stream beam convolution) of the CMB signal due to the pixelization of the map. With such, we can now easily incorporate this extra smoothing effects into our formalism by replacing our $B_{\ell(\text{eff})}^2$ with (see also eq. [5-9])

$$B_{\Pi\ell(\text{eff})}^2 \approx \overline{B}_{\Pi p\ell(\text{ms})}^2 \quad (8-8)$$

$$\approx \overline{B}_{p\ell(\text{ms})}^2 \Pi_{\ell(\text{ms})}^2 \quad (8-9)$$

$$\approx B_{\ell(\text{eff})}^2 \Pi_{\ell(\text{ms})}^2, \quad (8-10)$$

where $\overline{B}_{\Pi p\ell(\text{ms})}^2$ is the power spectrum of the $\overline{B}_{\Pi p}$ defined in equation (8-5), and $\Pi_{\ell(\text{ms})}^2$ is the power spectrum of the $\Pi(\mathbf{x})$ defined in equation (8-7). We note that in the limiting case where $\mathbf{x}_t = \mathbf{x}_{p\supset t}$, we have $\Pi_{p\ell m}$ equal to unity for all ℓ and m (since the multipole transform of $\delta(\mathbf{x})$ is unity), so the smoothing effects disappear, and we have exactly $B_{\Pi\ell(\text{eff})}^2 = B_{\ell(\text{eff})}^2$ (see eq. [8-10]). If the pixels do not have exactly the same shape, as in the case on any large patch of the sphere (e.g., pixelized by HEALPix, Gorski et al. 1999, or by Igloo, Crittenden & Turok 1998), then we can use equation (8-8) together with equation (8-5) to obtain $B_{\Pi\ell(\text{eff})}^2$. If the pixel beam or the pixel shape remains roughly the same for all pixels, then we can use equation (8-9) together with equations (5-9) and (8-7) to calculate $B_{\Pi\ell(\text{eff})}^2$.

If all the pixels have the same shape which is a regular square of size ς in radians, then we have

$$\Pi_{\ell(\text{ms})}^2(\varsigma) = \frac{8}{\pi} \int_0^{2\pi} d\phi \frac{\sin^2 [(\ell\varsigma \cos \phi) / 2] \sin^2 [(\ell\varsigma \sin \phi) / 2]}{\ell^4 \varsigma^4 (\cos^2 \phi) (\sin^2 \phi)}. \quad (8-11)$$

An accurate approximation to this result is

$$\Pi_{\ell(\text{ms})}^2(\varsigma) \approx \exp \left[-\frac{(\ell\varsigma)^{2.04}}{18.1} \right] [1 - 2.72 \times 10^{-2} (\ell\varsigma)^2]. \quad (8-12)$$

The accuracy of this fit is within 0.3% error for $\ell < 1.4\pi/\varsigma$. For example, if the pixel size is 5×5 square arcminutes (i.e., $\varsigma = 5$ arcminutes $\approx 1.45 \times 10^{-3}$ radians), then the above fit is at 99.7% accuracy for $\ell < 3024$.

9. NUMERICAL VERIFICATIONS

9.1. The pixel-beam expansion

In this and the following three subsections, we will employ an elliptic Gaussian beam with a short-axis FWHM of 5 arc-minutes and a long-axis FWHM of 20 arc-minutes, to demonstrate certain key points developed previously. We first investigate the pixel-beam expansion of a given pixel resulting from different scanning strategies, i.e., to investigate the dependence of the pixel-beam power spectrum (4-17) on the function $f(\beta)$, and to verify the results given in equation (4-20). We note that although those results are given for the average pixel-beam expansion, we expect the pixel-beam expansion to carry the same property since equation (4-7) has exactly the same form as equation (4-10). Figure 1 shows two different configurations of beam scanning on a given pixel. In case A, the pixel was hit twice by the same beam pattern, but with different orientations of a separation angle α . That is $f(\beta) \equiv [\delta(\beta) + \delta(\beta - \alpha)]/2$. We shall investigate the cases $\alpha = 15, 45$, and 90 degrees. In case B, the pixel was hit evenly in four different directions. That is $f(\beta) \equiv [\delta(\beta) + \delta(\beta - 45^\circ) + \delta(\beta - 90^\circ) + \delta(\beta - 135^\circ)]/4$.

Figure 2 shows the IOA of the pixel beams in cases A and B, as defined in equation (3-4). As one can see, the pixel beam has the largest asymmetry (largest ϖ_ℓ) when the pixel is hit by a beam with only one direction (the dashed line). When the pixel is hit by beams of two different directions (case A in Figure 1), the asymmetry decreases (ϖ_ℓ decreases) if the separation angle of the two directions α is closer to 90 degrees (see the dotted lines in Figure 2). When the pixel is scanned with four different directions (case B in Figure 1), the resulting effective beam is nearly symmetric ($\varpi_\ell \approx 0$) up to $\ell \sim 1000$, and has the lowest level of asymmetry (the smallest ϖ_ℓ).

Figure 3 shows the power spectra of the pixel-beam expansions with different scanning strategies. As we can see, the power spectrum of the pixel-beam expansion has a maximum given by equation (3-2) (see also eq. [4-19]), when the pixel was scanned with only one direction. On the other hand, the power spectrum of the pixel-beam expansion has a minimum given by equation (3-3) (see also eq. [4-18]), when the pixel was scanned evenly in all directions (note that the dot-dashed line in Figure 3 almost coincides with the solid line). This verifies our results given in equation (4-20). By comparing Figure 3 with Figure 2, we also learn that there is a strong correlation between ϖ_ℓ and the B_ℓ^2 of a pixel—when the pixel is scanned by a same beam pattern with more different directions, the level of the effective beam asymmetry (ϖ_ℓ) decreases, and so does the power spectrum of the pixel-beam expansion (B_ℓ^2).

We also note that according to equation (6-5), the IOA of the original time-stream

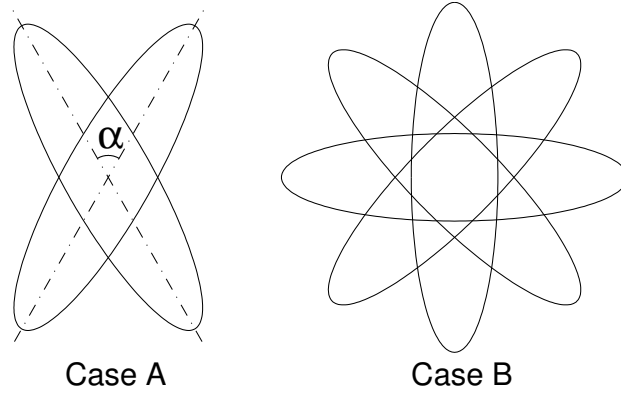


Fig. 1.— Beam configurations on a given pixel, resulting from different scanning strategies.

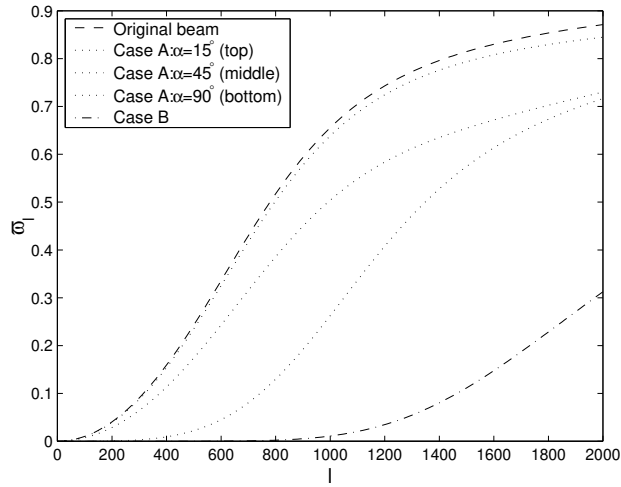


Fig. 2.— Indices of asymmetry of the pixel-beam expansions, as functions of the multipole number l .

beam B_0 (the dashed line in Fig. 2) also tells us beyond what ℓ we need to worry about the asymmetry of the beam. For example, when $\ell \lesssim 600$, we see that $\varpi_\ell \lesssim 0.3$, giving $\varpi_\ell^2/2 \lesssim 0.05$. This means that if we simply use the $B_{0\ell(\text{mid})}^2 = 2/[B_{0\ell(\text{ms})}^{-2} + B_{0\ell(\text{sm})}^{-2}]$ (eq. [6-4]) as the $B_{\ell(\text{eff})}^2$ in the formalism (5-10), then the maxima error in the final C_ℓ estimates is guaranteed to be within about $\pm 5\%$ for $\ell \lesssim 600$.

9.2. The pixel-pixel beam expansion

We now use the elliptic Gaussian beam of 5 by 20 arcminutes to verify some important results in section 5—mainly equation (5-9). Consider a square map of size $10^\circ \times 10^\circ$, with a square pixel size of 5 arcminutes. Referring to equation (5-6) with such a map, Figure 4 shows how φ_0 is distributed at each Δx . In the figure, each dot labels the $(\Delta x, \varphi_0)$ that is sampled by the map. As one can see, φ_0 is nearly uniformly distributed for any given Δx , except when Δx is close to the boundaries constrained by the pixel and field sizes. Because of this nearly uniform distribution, we achieved equation (5-9) from equation (5-6).

More precisely, we carried out equation (5-6) to obtain $B_{\ell(\text{eff})}^2$, and calculated the right hand side of equation (5-9) to obtain $B_{\ell(\text{ms})}^2$. Here we have used the elliptic Gaussian beam directly as the $\widetilde{B}_p(\mathbf{k}) \equiv \overline{B}_{p\ell m}$ in the due calculations. We found that $B_{\ell(\text{ms})}^2$ agrees with $B_{\ell(\text{eff})}^2$ with more than 99% accuracy for $\ell = 0\text{--}2000$.

We have also calculated the average deviation σ_ℓ of $B_{pp'\ell}^2$ from $B_{\ell(\text{eff})}^2$ for each individual pixel pair, using equation (5-13). The result is shown in Figure 5. First, we see many spikes in σ_ℓ . This is due to the zeros of the Bessel function J_0 , which appears at the bottom of equation (5-13). These spikes should be neglected, as in reality no such singularities appear in our analysis pipeline. We note that these spikes have the same origin as those presented in Hanany et al. (1998), where a similar situation was considered. Second, as addressed previously, although the σ_ℓ obtained from equation (5-13) can be as large as comparable to unity, the real errors in the final C_ℓ estimates by using the formalism (5-11) with the approximation (5-9) will be much smaller than this value. This is because the σ_ℓ here tells only the mean discrepancy of $B_{\ell(\text{eff})}^2$ for each individual pixel pair, and may average out when all pixel pairs come into account in the likelihood analysis. In section 9.5, we will numerically justify this and thus the accuracy of employing equation (5-11) with (5-9).

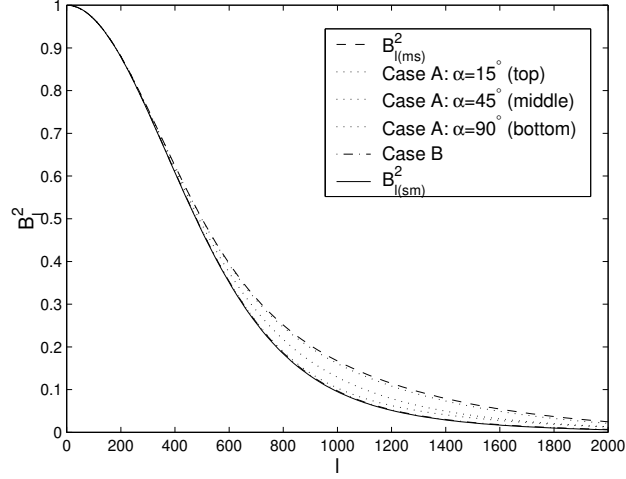


Fig. 3.— Power spectra B_ℓ^2 of the pixel-beam expansions with different scanning strategies.

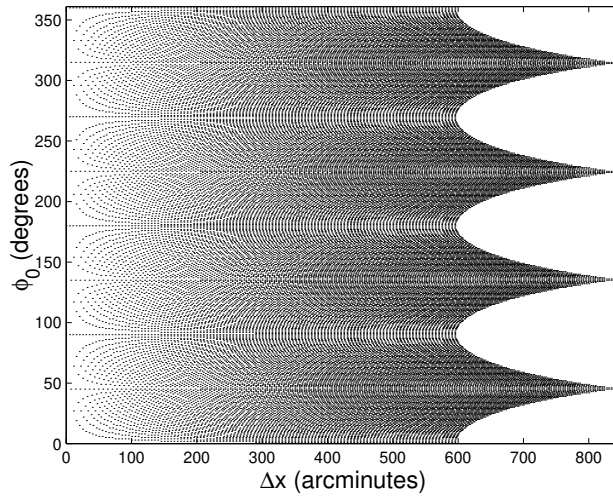


Fig. 4.— Distribution of φ_0 as a function of Δx . Each dot labels the $(\Delta x, \varphi_0)$ that is sampled by a square map of $10^\circ \times 10^\circ$, with a pixel size of 5 arcminutes.

9.3. Uncertainties from beam measurement

In this section, we will numerically verify the results in section 7. First, we use a symmetric Gaussian beam with a FWHM of 10 arcminutes, to investigate the approximation $\Delta_{C_\ell(\text{G})}^*$ given by (7-8), as a comparison to the exact result $\Delta_{C_\ell(\text{G})}$ given by (7-5). Here we take the uncertainty in the beam measurement to be $\epsilon = 10\%$ (eq. [7-1]). As one can see in Figure 6, the approximation breaks down towards the limit $\ell_{(\text{G})}^*$ given by equation (7-9). For $\ell \ll \ell_{(\text{G})}^*$, the approximation $\Delta_{C_\ell(\text{G})}^*$ reproduces the correct result $\Delta_{C_\ell(\text{G})}$. By comparing $\Delta_{C_\ell(\text{G})}^*$ and $\Delta_{C_\ell(\text{G})}$, we calculate the 10% accuracy limit $\ell_{(\text{G}:10\%)}^*$ (the dot-dashed line), at which $\Delta_{C_\ell(\text{G})}^*/\Delta_{C_\ell(\text{G})} - 1 = 10\%$. In addition, by varying the value of ϵ between $\pm 20\%$, we obtain the result presented in equation (7-10). That is, for a symmetric Gaussian beam with an uncertainty of ϵ in size, the approximation (7-8) for the resulting uncertainty in C_ℓ is accurate within 10% error for $\ell < \ell_{(\text{G}:10\%)}^* = (0.44 + 0.8|\epsilon|)\ell_{(\text{G})}^*$.

Now we investigate the case where the beam is asymmetric. We use an elliptic Gaussian beam, whose long- and short-axis FWHM's are 20 and 5 arcminutes respectively. This beam is first convolved onto a simulated CMB map of size $10^\circ \times 10^\circ$, with a pixel size of 10 arcminutes. The underlying cosmology is an inflationary model with $(\Omega_b, \Omega_{\text{cdm}}, \Omega_\Lambda, n, h) = (0.07, 0.61, 0.23, 1, 0.60)$, normalized to the COBE DMR. A random Gaussian noise of $100\mu K$ is then added into each pixel. We call this simulation (1). We repeat the same procedure again except that this time the beam size is increased by 10%, i.e., $\epsilon = 10\%$, to obtain a simulation (2), where the CMB and noise realizations are exactly the same as those used in simulation (1). We then analyze both simulations using the procedure outlined in section 2, with the approximation (5-11). The resulting uncertainty in C_ℓ can thus be calculated using equation (7-4) as

$$\Delta_{C_\ell(\text{a})} = \frac{C_{\ell(2)}}{C_{\ell(1)}} - 1, \quad (9-1)$$

where the subscripts (1) and (2) indicate results from the two simulations. The results are shown as crosses in Figure 7. Also plotted is the result using equation (7-5) (the solid line), which we label with a subscript (b). It is obtained directly by varying the beam shape with $\epsilon = 10\%$. As one can see, the crosses are highly consistent with the solid line. This means, first, that the asymmetry of the beam does not affect our result given by equation (7-5). Second, the banding of ℓ does not affect the result, so we can use equation (7-5) as an estimate for the uncertainty in the band power C_b resulting from that in the beam measurement. This is also an important support to the fact that the banding of ℓ does not affect the general relation $C_\ell \propto B_\ell^{-2}$ (see eqs. [5-10] and [5-11]). We have also verified that the sizes of the error bars in the C_ℓ estimates between simulations (1) and (2) do not change by more than 4% for $\ell < 1200$. Thus we know that when Δ_{C_ℓ} is small, the uncertainty in the beam shape measurement does not affect the sizes of error bars significantly, but does affect

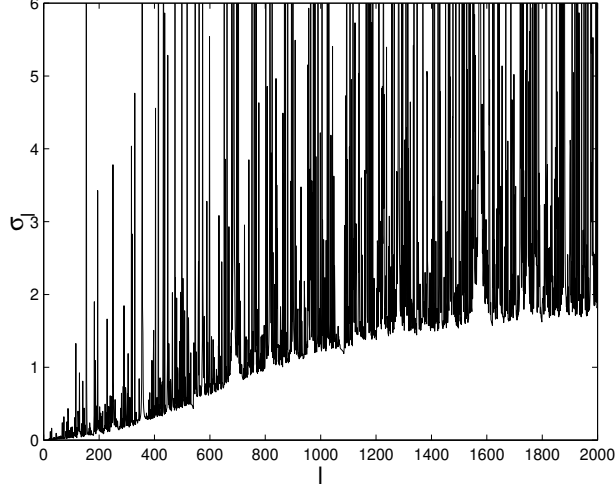


Fig. 5.— Mean discrepancy σ_ℓ of $B_{pp'\ell}^2$ from $B_{\ell(\text{eff})}^2$ for each individual pixel pair.

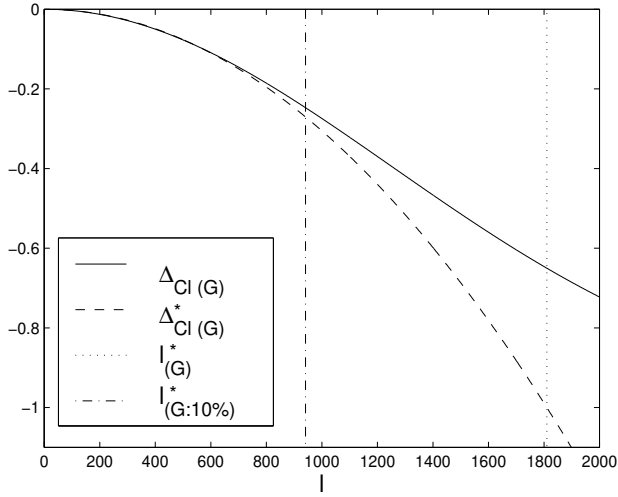


Fig. 6.— Uncertainty in the C_ℓ (solid line; given by eq. [7-5]), resulting from an uncertainty of $\epsilon = 10\%$ in the beam shape measurement of a Gaussian beam with a FWHM of 10 arcminutes. Also plotted is the approximation (7-8) (dashed line). The dotted vertical line indicates the limit of the approximation $\ell_{(G)}^*$ given by equation (7-9), while the dot-dashed vertical line shows the 10% accuracy limit $\ell_{(G:10\%)}^*$, which is well fitted by equation (7-10).

the amplitudes of the C_ℓ estimates. On the other hand, when Δ_{C_ℓ} is large (comparable to one), the signal to noise ratio may be affected and so may the error bar sizes.

9.4. Deconvolution of the pixel smoothing

We now test the formalism of deconvolving the smoothing effect due to the pixelization of a map. This is to verify equation (8-9), with equation (8-12) as an approximation in cases where the pixels are regular squares. We consider a square CMB map of size $10^\circ \times 10^\circ$, with regular-square pixels of size 10 arcminutes. We first simulate a time-stream of the CMB signal γ_t , that is convolved with an elliptic Gaussian beam of 5 by 20 arcminutes in FWHM (same as the one used in previous sections). For each temporal sample, we then add Gaussian random white noise n_t with 5% in RMS amplitude. In this run, we require the temporal samples to be exactly at the centers of each pixels, i.e., $\mathcal{N}_t = \mathcal{N}_p$ and $\mathbf{x}_t = \mathbf{x}_{p \ni t}$, such that $m = d$ (see eq. [2-5]). We call this simulation (0). In a second run, the procedure is the same except that the CMB temporal samples now have offsets with respect to the centers of each pixels, i.e., $\mathcal{N}_t = \mathcal{N}_p$ but $\mathbf{x}_t \neq \mathbf{x}_{p \ni t}$ with $\mathbf{x}_t - \mathbf{x}_{p \ni t}$ randomly distributed within a square of size 10 arcminutes. We call this simulation (1). In third, fourth, and fifth runs, the procedures are the same as simulation (1), except that the numbers of temporal samples in each pixels are now 3, 10, and 200 (i.e., $\mathcal{N}_t = 3\mathcal{N}_p$, $10\mathcal{N}_p$, and $200\mathcal{N}_p$) respectively, instead of one. We denote these as simulations (3), (10), and (200) respectively. All these runs are then analyzed in the same way, using the procedure outlined in section 2, with the approximation (5-11) and $B_{\ell(\text{eff})}^2 = \overline{B}_{p\ell(\text{ms})}^2$ (eq. [5-9]). Therefore the ratio

$$\frac{C_{\ell(j)}}{C_{\ell(0)}}, \quad j = 1, 3, 10, 200, \quad (9-2)$$

will quantify the smoothing effect due to the pixelization of the map. We plot this ratio in Figure 8, as a comparison to the $\Pi_{\ell(\text{ms})}^2$ given in equation (8-12).

As one can see and expect, the smoothing effect approaches the top-hat-window approximation when the number of temporal samples per pixel increases. When it is larger than 10, as in most real situations, the top-hat-window approximation appears to be a good one. Also plotted at the bottom-left corner is the $\Pi(\mathbf{x})$ given by equation (8-7) for $j = 10$. The nearly uniform distribution of $\mathbf{x}_{p \ni t} - \mathbf{x}_t$ shows the appropriateness of the top-hat-window approximation. Thus we have verified that the approximation (8-9), with equation (8-12) for cases where pixels are regular squares, is indeed a good approximation. For an obvious mathematical reason (see sec. 8), we know that this formalism can be further extrapolated for cases where pixels do not have regular shapes but the time-stream beams have roughly

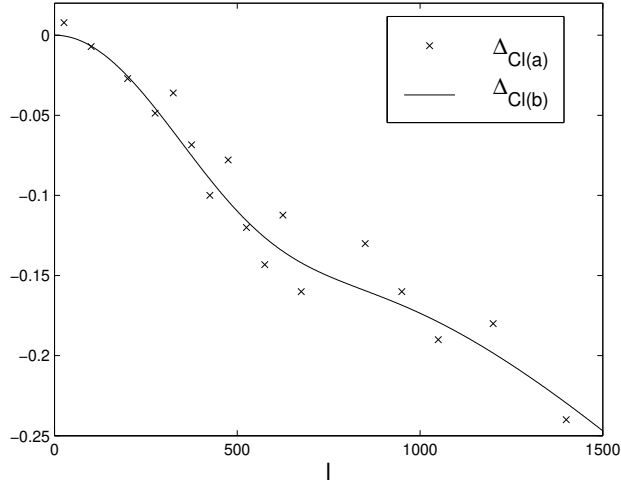


Fig. 7.— Uncertainty in the C_ℓ resulting from that in the beam measurement. The horizontal axis is the multipole number ℓ . The crosses, $\Delta_{C_\ell(a)}$, are results based on simulations using equation (7-4) (or eq. [9-1]), while the solid line, $\Delta_{C_\ell(b)}$, is obtained directly from the beam shape using equation (7-5). An elliptic Gaussian beam, with long- and short-axis FWHM's of 20 and 5 arcminutes respectively, is used. The uncertainty in the beam shape is $\epsilon = 10\%$.

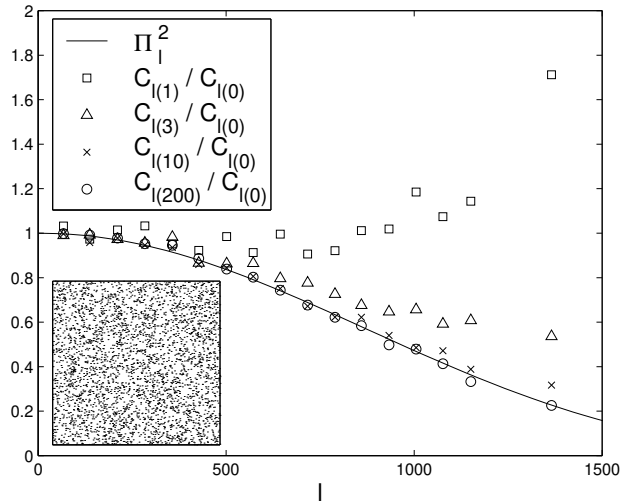


Fig. 8.— Smoothing effect due to the pixelization of a CMB map. The ratios $C_{\ell(j)}/C_{\ell(0)}$ are compared to the approximated smoothing window $\Pi_{\ell(ms)}^2$, with $j = 1, 3, 10, 200$ representing the number of temporal samples per pixel in different runs. The horizontal axis is the multipole number ℓ . The square at the bottom-left corner shows the $\Pi(\mathbf{x})$ for $j = 10$.

the same shape. In such cases, equation (8-7) can be employed to obtain the $\Pi_{\ell(\text{ms})}^2$ for the use of equation (8-9).

9.5. The MAXIMA experiment

In this section we demonstrate the application of our formalism using the data from the MAXIMA-1 experiment (H00). Figure 9 shows the antenna patterns B_i ($i = 1, 2, 3, 4$) for the four photometers used in the analysis of the MAXIMA-1 data. Details of the measurements of these beam shapes are given in H00. As one can see, the beams are more symmetric towards their centers.

Figure 10 shows the level of asymmetry of the beams. The dotted lines are the IOA $\varpi_{i\ell}$ of each individual beam B_i (eq. [3-4]), and the solid line is the IOA of the noise-weighted combination of all of them, i.e., the ϖ_ℓ of the average pixel-beam expansion $\overline{B}_{p\ell m}$ (see eqs. [4-10], [4-11], and [4-12]). The dashed line is the IOCA \mathcal{W}_ℓ from all B_i (eq. [3-5]). Here the relative weight of each beam is $\zeta_1 : \zeta_2 : \zeta_3 : \zeta_4 = 64 : 64 : 81 : 36$ (see eq. [3-8] and H00). As we can see, the beams are nearly symmetric ($\mathcal{W}_\ell, \varpi_\ell \approx 0$) at low ℓ , but less so at larger ℓ . At $\ell \lesssim 800$, which is the range of ℓ discussed in H00, the asymmetry is less than 15%. The figure also confirms the fact that the ϖ_ℓ of $\overline{B}_{p\ell m}$ must be equal to or smaller than \mathcal{W}_ℓ , although the individual $\varpi_{i\ell}$ may be larger than \mathcal{W}_ℓ (see sec. 3).

The top panel of Figure 11 shows the pixel-pixel beam expansions, $B_{\ell(\text{eff})}^2$ of equation (5-4). The dotted lines are the results of the individual beams, which are denoted here as $B_{\ell(i)}^2$. The solid line is the result of the combined beam, which is denoted here as $B_{\ell(c)}^2$. Also plotted are the $B_{\Sigma\ell(\text{sm})}^2$ (eq. [3-6]) and $B_{\Sigma\ell(\text{ms})}^2$ (eq. [3-7]). Here we have used the MAXIMA-1 scans and a pixel size of 5×5 square arcminutes. The bottom panel compares all the above B_ℓ^2 to $B_{\Sigma\ell(\text{mid})}^2 = 2/[B_{\Sigma\ell(\text{sm})}^{-2} + B_{\Sigma\ell(\text{ms})}^{-2}]$ (eq. [6-6]), with all line styles the same as indicated in the top panel.

We first see that all the B_ℓ^2 have close shapes, with considerable discrepancies only at high ℓ where the amplitude of B_ℓ^2 is small. Second, the bottom panel confirms that the $B_{\ell(c)}^2$ is well constrained by $B_{\Sigma\ell(\text{sm})}^2$ and $B_{\Sigma\ell(\text{ms})}^2$ (see eqs. [4-22] and [5-9]), whose fractional difference is roughly given by \mathcal{W}_ℓ^2 (see definition [3-5]), square of the dashed line in Figure 10. Hence according to equation (6-7) and Figure 10, we know that the maximum fractional error in the final C_ℓ estimates by taking $B_{\ell(\text{eff})}^2 = B_{\Sigma\ell(\text{mid})}^2$ for the MAXIMA-1 data will be about $\mathcal{W}_\ell^2/2 \approx 5\%$ for $\ell < 2000$. Although this is already a small error, we still take $B_{\ell(\text{eff})}^2 = B_{\ell(c)}^2$ in the MAXIMA-1 data analysis for higher accuracy. The difference between $B_{\ell(c)}^2$ and $B_{\Sigma\ell(\text{mid})}^2$ is manifested by the non-zero solid line in the bottom panel of Figure 11.

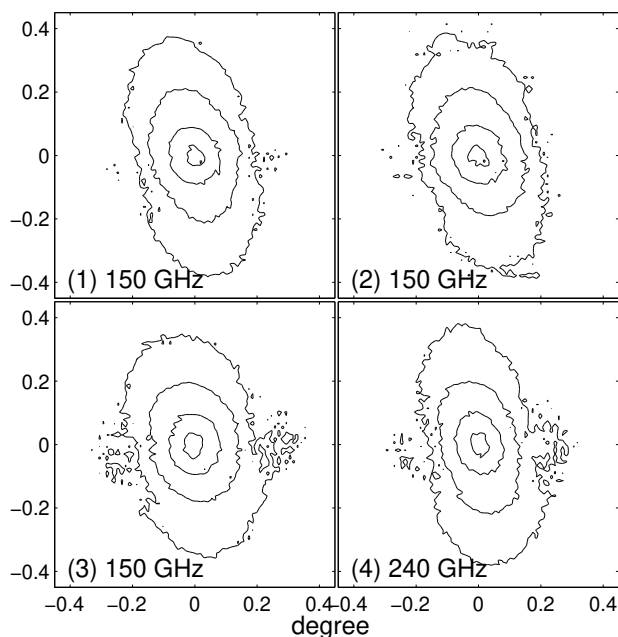


Fig. 9.— Iso-height contours of the beams used in the analysis of the MAXIMA-1 data (H00). Contours correspond to the 90%, 50%, 10%, and 1% amplitude levels.

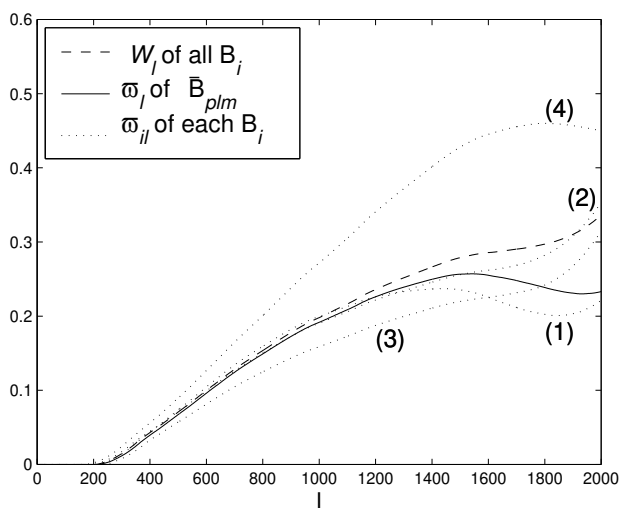


Fig. 10.— Indices of asymmetry of MAXIMA-1 beams (dotted lines) and of the noise-weighted combination (solid line). Also plotted is the index of combined asymmetry of all MAXIMA-1 beams (dashed line).

In addition, we have also verified that for both the individual and the combined beams, the approximation $B_{\ell(\text{eff})}^2 \approx \overline{B}_{p\ell(\text{ms})}^2$ (eq. [5-9]) is accurate within 1% error for $\ell < 2000$. This means that in general situations one can simply use $\overline{B}_{p\ell(\text{ms})}^2$ as the $B_{\ell(\text{eff})}^2$ to avoid the complicated procedure of evaluating the $B_{\ell(\text{eff})}^2$ of equation (5-4) with (5-1).

Using equation (5-11) with the $B_{\ell(\text{eff})}^2$ replaced with $\overline{B}_{p\ell(\text{ms})}^2 \Pi_{\ell(\text{ms})}^2$ (see eq. [8-9]), we tested to what extent our formalism biases the CMB angular power spectrum estimate. We simulated a CMB signal γ_t in the time domain. Each time-domain point is allocated the pointing coordinates of the MAXIMA-1 scan and the signal is convolved with the measured MAXIMA-1 beams. In the MAXIMA-1 scan most pixels are scanned in two different directions. We then added time domain noise n_t which has the MAXIMA-1 characteristics: an overall white noise, with a $1/f$ behavior at low frequencies due to the receiver response and a power law at high frequencies due to the electronic filtering. We call this ($d_t = \gamma_t + n_t$) simulation (a). We repeated the procedure to generate simulation (b), in which the CMB signal is convolved with a symmetric beam whose power spectrum is identical to $\overline{B}_{p\ell(\text{ms})}^2$. Both simulations were then analyzed in exactly the same way, using the procedure described in section 2, with the approximation (5-9), (5-11), (8-9), and (8-12). Here we have employed the quadratic estimator (Bond et al. 1998) to estimate the power spectra $C_{\ell(\text{a})}$ and $C_{\ell(\text{b})}$ for simulations (a) and (b), respectively. (The quadratic estimator was implemented by two independent codes, one of which is that by Borrill (1999) and the other by the first author, and yielded consistent results with less than 0.1% discrepancy.) We then use

$$\lambda_\ell = \frac{C_{\ell(\text{a})} - C_{\ell(\text{b})}}{\tau_{\ell(\text{a})}}, \quad (9-3)$$

where $\tau_{\ell(\text{a})}$ is the error bar associated with $C_{\ell(\text{a})}$, to quantify how much our formalism biases the C_ℓ estimates. The entire procedure is repeated six times to yield six independent λ_ℓ . In Figure 12 we plot λ_ℓ Vs. ℓ for the six realizations, the means of these six sets of λ_ℓ , and the standard deviations. As we can see, the means are within 10% of the error bar sizes $\tau_{\ell(\text{a})}$ of each $C_{\ell(\text{a})}$.

With the same scan strategy, pixelization scheme, and noise property, we repeated the same test using an extremely elliptic Gaussian beam of 5 by 20 arcminutes in FWHM (the one we used previously). We found again that the means of λ_ℓ are within 10% of the error bar sizes $\tau_{\ell(\text{a})}$ for $\ell < 2000$. We therefore conclude that our formalism does not bias the C_ℓ estimates.

Finally, we consider the uncertainties in the C_ℓ estimates resulting from uncertainties in the measurement of the beam shape, as discussed in section 7. H00 quoted an uncertainty of $\epsilon = \pm 5\%$ in the measurement of the MAXIMA-1 beams. The dominant contributors to this uncertainty are of the type discussed in section 7 (eq. [7-1]) and contribute to an

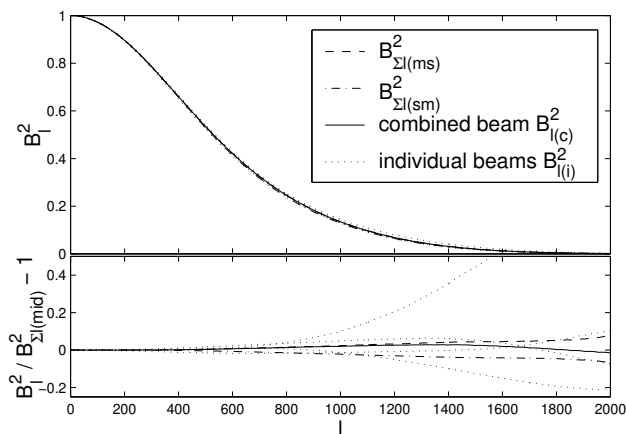


Fig. 11.— Pixel-pixel beam expansions $B_{\ell(\text{eff})}^2$ of MAXIMA-1 beams and their noise weighted combination (top panel), and a comparison of these results (bottom panel; see text). Also plotted are the $B_{\Sigma\ell(\text{sm})}^2$ and $B_{\Sigma\ell(\text{ms})}^2$.

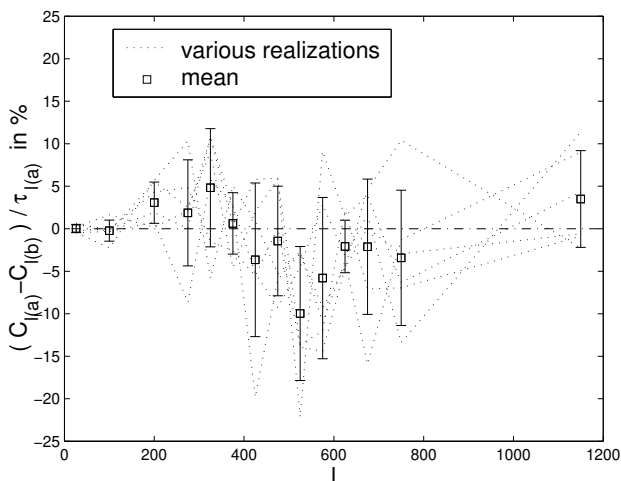


Fig. 12.— Results of simulations testing whether our formalism biases the CMB angular power spectrum estimate. The simulations use the MAXIMA-1 scan strategy. Plotted is the difference between angular power spectra calculated from simulations that have a CMB signal convolved with symmetric and MAXIMA-1 (asymmetric) beams. The difference is normalized by the errors of one of the power spectra (see the text). The dotted lines show results using different realizations of the CMB signal and the noise. The boxes are the averages and error bars are the standard deviations.

uncertainty in the C_ℓ estimates that is correlated between different ℓ bins. Substituting this value into equation (7-5) and using the $\overline{B}_{p\ell(\text{ms})}^2$ we calculated previously, we obtain the estimated uncertainties $\Delta_{c_\ell} = dC_\ell/C_\ell$ in the C_ℓ estimates. Figure 13 shows the results. As one can see, the estimated uncertainties in the C_ℓ estimates are $|\Delta_{c_\ell}| < 6\%$, 17% , and 40% for $\ell < 500$, 1000 , and 1500 respectively. When we include the MAXIMA-1 window-functions of ℓ , we find that for the bands used in H00, the beam size uncertainty causes less than 4% and 11% uncertainty in the C_ℓ estimates for $\ell < 410$ and 785 , respectively.

10. DISCUSSION AND CONCLUSION

First we summarize the treatment of asymmetric beams for yielding accurate C_ℓ estimates in CMB anisotropy experiments:

1. Based on the measured individual beam pattern B_0 , one calculates the IOA, $\varpi_{0\ell}$, using equation (3-4), to quantify the level of asymmetry of the beam on different angular scales. If $\varpi_{0\ell}^2/2$ is below the tolerated maximum error for the C_ℓ estimates at the ℓ range of interest (see eq. [6-5]), then one takes $B_{\ell(\text{eff})}^2 = B_{0\ell(\text{mid})}^2$ as given by equation (6-4) (see also eqs. [3-2] and [3-3] for definitions), and goes to step 4, otherwise step 2. The resulting errors in the C_ℓ estimates by taking $B_{\ell(\text{eff})}^2 = B_{0\ell(\text{mid})}^2$ is quantified by equation (6-5). Similarly, when combining data from photometers of different beam shapes, one first calculates the IOCA \mathcal{W}_ℓ using equation (3-5), and then employs condition (6-7) for the same check. If $\mathcal{W}_\ell^2/2$ is small, then one takes $B_{\ell(\text{eff})}^2 = B_{\Sigma\ell(\text{mid})}^2$ as given by equation (6-6) and goes to step 4, otherwise step 2.
2. One checks if all the pixels have the same shape, and if the time-stream beam B_t remains unchanged throughout the entire observation. If either or both of these hold, then one goes to step 3. Otherwise, one calculates $B_{\Pi\ell(\text{eff})}^2 \approx \overline{B}_{\Pi p\ell(\text{ms})}^2$ using equations (4-11), (4-12), (8-5), and (8-8), and then go to step 5.
3. One calculates the average pixel-beam expansion $\overline{B}_{p\ell m}$ using equations (4-10), (4-11), and (4-12). We note that equation (4-10) also works for combining data sets from different photometers with different beam shapes, as long as the noise level μ_t is well taken into account. One then calculates the power spectrum $\overline{B}_{p\ell(\text{ms})}^2$ of $\overline{B}_{p\ell m}$ (see eq. [4-15]). This can be implemented using the form of equation (4-17) to save computation time, i.e. one calculates the weighting function $f(\beta)$ first, with discretized β , and then the $\overline{B}_{p\ell(\text{ms})}^2$ accordingly. A useful check of this result is provided by equation (4-20) or (4-21). One thus takes $B_{\ell(\text{eff})}^2 \approx \overline{B}_{p\ell(\text{ms})}^2$ according to equation (5-9), and goes to the next step.

4. To incorporate the smoothing effect due to the pixelization of the map, one employs equation (8-10) to obtain the pixel-pixel beam expansion $B_{\Pi\ell(\text{eff})}^2 \approx B_{\ell(\text{eff})}^2 \Pi_{\ell(\text{ms})}^2$. In general, the associated $\Pi_{\ell(\text{ms})}^2$ can be obtained by multipole transforming the $\Pi(\mathbf{x})$ that is defined in equation (8-7). If all pixels are regular squares, one can instead use the convenient result in equation (8-12).
5. One then employs equation (2-5) to make a map, and equations (2-6) (or alternatives like the quadratic estimator), (2-7), (2-9), and (5-11) to estimate the ℓ -banded power spectrum C_b . We note that in equation (5-11), one replaces the $B_{\ell(\text{eff})}^2$ with the $B_{\Pi\ell(\text{eff})}^2$ obtained previously.
6. The uncertainties in the final band power C_b resulting from the uncertainties in the beam measurement can then be calculated using equation (7-5). In cases where the beam has a Gaussian form, one can instead use equation (7-8) with the condition (7-10) to estimate the uncertainties. These uncertainties need to be incorporated in both the final C_ℓ estimates and the estimates of cosmological parameters.

In previous sections, we developed the above treatment for asymmetric beams in order to obtain accurate C_ℓ estimates at smaller angular scales. This treatment employs the symmetric-beam approximation, where the originally asymmetric beams are symmetrized. The smoothing effects due to the pixelization of the CMB map are taken into account. The resulting uncertainties in the C_ℓ estimates due to the uncertainties in the beam measurement are also estimated. In addition, we derived the conditions under which one needs to employ this formalism to account for the asymmetry of beams. We demonstrated certain key points by using a simulated highly elliptic beam, and the beams and data of the MAXIMA-1 experiment, where the asymmetry is mild. In particular, we showed that in both cases the formalism does not bias the final C_ℓ estimates.

In spite of the power of the new formalism in dealing with various practical situations where the beams are not symmetric, we should note that it may break down under certain circumstances. First, if the sky patch to be analyzed has an extremely irregular shape, then the important result $B_{\ell(\text{eff})}^2 \approx \overline{B}_{p\ell(\text{ms})}^2$ (eq. [5-9]) may be invalid due to the nonuniform distribution of φ at each given Δx (see eqs. [5-6] and [5-7]). Nevertheless, the formalism as a whole is still valid in this case, because one can instead employ equation (5-4), $B_{\ell(\text{eff})}^2 = \langle B_{pp'\ell}^2 \rangle$, although it is more computationally expensive. Second, if the total numbers of the pixels (\mathcal{N}_p) and of the temporal samples (\mathcal{N}_t) are not large, then some statistical averages taken in the formalism may not be appropriate (e.g., eqs. [4-8], [5-4], [5-9], and [8-5]). This will cause the violation of some main results like equations (5-9), (8-8), and (8-10). However, since the \mathcal{N}_p and \mathcal{N}_t are not large in this case, one can always employ the full treatment

of asymmetric beams as described by equation (2-8). The main results of our formalism are needed only when \mathcal{N}_p and \mathcal{N}_t are large enough to cause computational difficulty in implementing equation (2-8). We note that even in the full treatment of asymmetric beams, our results in dealing with the extra convolution effects due to the pixelization of the map (see sec. 8) can still be employed. Third, the main results of our formalism have assumed that the experimental noise in the temporal samples is independent from each other (i.e., the white-noise assumption; see eq. [4-4]), so these results may not be suitable for experiments that have strongly correlated noise. Nevertheless, as argued in the appendix, most experiments should have only mild departure from the white noise, and this departure does not affect our main results. In general, one can use condition (A10) or equation (A11) to choose a proper pixel size, so that the white-noise approximation is still appropriate. As we have also numerically verified, our formalism does not induce any bias in the final C_ℓ estimates in the presence of the nonwhite noise in the MAXIMA-1 data. Even if the experimental noise is extremely nonwhite, we can still deal with asymmetric beams by employing the general results in our formalism. This means the use of equation (8-2), together with equations (8-8) and (5-11) for the C_ℓ estimation.

In conclusion, we have proposed a complete and well justified formalism for the data analysis of CMB anisotropy experiments. This formalism is very flexible and therefore well suited to a wide spectrum of circumstances, especially when the experimental beams are not symmetric. No matter how irregular the beams are, the formalism always provides a both computationally economical and statistically plausible way to estimate the angular power spectrum of the CMB. We expect this formalism to be useful not only for the small-field experiments, but also for the full-sky experiments like PLANCK and MAP.

JHPW and AHJ acknowledge support from NASA LTSA Grant no. NAG5-6552 and NSF KDI Grant no. 9872979. PGF acknowledges support from the RS. BR and CDW acknowledge support from NASA GSRP Grants no. S00-GSRP-032 and S00-GSRP-031. MAXIMA is supported by NASA Grants NAG5-3941, NAG5-4454, by the NSF through the Center for Particle Astrophysics at UC Berkeley, NSF cooperative agreement AST-9120005. The data analysis used resources of the National Energy Research Scientific Computing center which is supported by the Office of Science of the U.S. Department of Energy under contract no. DE-AC03-76SF00098.

A. Non-white noise

In this appendix, we consider the pixel-beam expansion $B_{p\ell m}$ (eq. [4-3]) in the case where the noise is not white (violation of eq. [4-4]), i.e., when it is correlated between pixels. We shall show that even in this case, for the purposes of determining $B_{p\ell m}$ and thus the pixel-pixel beam expansion, the white-noise approximation (4-4) is still appropriate under certain conditions, which are generally satisfied by practical situations.

We start with the general requirement (4-3). In the real space, this equation is equivalent to

$$A_{p't'}^T N_{t't}^{-1} A_{tp} B_p(\mathbf{x}) = A_{p't'}^T N_{t't}^{-1} B_t(\mathbf{x}). \quad (\text{A1})$$

We note that the center of the $B_t(\mathbf{x})$ here is not at $\mathbf{x} = 0$, but at the location \mathbf{x}_t of the temporal sample at time t . The similar also applies to the $B_p(\mathbf{x})$. Thus we see that with a given pixelization scheme (and thus given A_{tp}), the relation between B_p and B_t depends only on the property of $N_{t't}$.

In most experiments, the temporal Fourier transform $\tilde{N}(f)$ of $N_{t't}$ in the frequency f domain usually has the following structure: a ‘ $1/f$ ’ behavior below f_1 due to the receiver response, a power law above f_h due to the electronic filtering, and a white noise of amplitude μ^2 (c.f. eq. [4-4]) between f_1 and f_h . Since the temporal Fourier transform $\widetilde{N^{-1}}(f)$ of $N_{t't}^{-1}$ is simply the inverse of $\tilde{N}(f)$, we can approximate a usual $\widetilde{N^{-1}}(f)$ as

$$\widetilde{N^{-1}}(f) \approx \mu^{-2} [H(f; f_h) - H(f; f_1)], \quad (\text{A2})$$

where μ^2 is the amplitude of the white noise part in $\tilde{N}(f)$, and $H(f; f_n)$ ($n = h, 1$) is a top-hat window function:

$$H(f; f_n) = \begin{cases} 1 & \text{for } |f| \leq f_n, \\ 0 & \text{for } |f| > f_n, \end{cases} \quad n = h, 1. \quad (\text{A3})$$

Thus in the real space we have

$$N_{t't}^{-1} \approx N_{ht't}^{-1} - N_{lt't}^{-1}, \quad (\text{A4})$$

where

$$N_{nt't}^{-1} = \mu^{-2} \text{sinc}(4\pi|t - t'|f_n), \quad n = h, 1. \quad (\text{A5})$$

Here we have used the usual definition $\text{sinc}(x) = 2 \sin(x/2)/x$. Therefore, to test if the white-noise approximation (see eqs. [4-4] and [8-3]) is appropriate, we can substitute $N_{ht't}^{-1}$ and $N_{lt't}^{-1}$ separately as the $N_{t't}^{-1}$ into equation (A1), and see if the resulting equation is consistent with the result (8-3). We may thus derive the conditions under which the result (8-3) is a good approximation even if the noise is not white.

We first consider the first term $N_{ht't}^{-1}$ in equation (A4), i.e. the effect from the high-frequency cut at f_h . In the white-noise case, the first term becomes $\lim_{f_h \rightarrow \infty} N_{ht't}^{-1}$, which is a Dirac Delta along the t and t' directions with a peak centered at $t = t'$. The fact that the width of this peak is zero means that the correlation time of the temporal scan is zero, so that each sample is independent and a pixel is related to only the temporal hits inside the pixel, giving the form (8-3). On the other hand, in cases where f_h is finite, the width of this central peak (the distance between the first zeros of $N_{ht't}^{-1}$ from $t = t'$ along the t or t' direction) is broadened (when compared to the white-noise case) from zero to $\delta t_h = 1/f_h$ (see eq. [A5]). This means that when the noise is white but with a cut-off beyond f_h , the correlation time of the temporal samples will be increased from zero to the order of $\delta t_h = 1/f_h$. Therefore, as long as the correlation time $\delta t_h = 1/f_h$ is well below the time required to scan across a pixel, the pixel will have no significant correlation with the temporal hits that are outside the pixel. In other words, the white-noise approximation (8-3) holds as long as

$$\frac{\delta x_p}{\delta x_t} \gg \frac{\delta t_h}{\delta t} = \frac{1}{f_h \delta t}, \quad (\text{A6})$$

where δx_p is the pixel size, δx_t is the spacing on the sky of the temporal samples, and δt is the integration time of each sample. Although δx_t is not a constant in general, its order in a single experiment normally remains the same.

Following a similar line of logic, we now consider the second term $N_{lt't}^{-1}$ in equation (A4), i.e. the effect from the low-frequency cut at f_l . In the white-noise case, the second term becomes $\lim_{f_l \rightarrow 0} N_{lt't}^{-1} = \mu^{-2}$, which is a constant along both the t and t' directions. This allows us to simplify equation (A1) as

$$\sum_p \mathcal{N}_{t \in p} B_p(\mathbf{x}) = \sum_t B_t(\mathbf{x}), \quad (\text{A7})$$

where $\mathcal{N}_{t \in p}$ is the number of temporal samples in the pixel p . Thus we see that equation (8-3) automatically fulfills the above requirement. On the other hand, in cases where f_l is finite, the $N_{lt't}^{-1}$ will remain constant along the t or t' direction from $t = t'$ out to about $|t - t'| = \delta t_l = 1/2f_l$ (the first zeros), beyond which it begins to decay away as power law with oscillations (see eq. [A5]). This means that when f_l is not zero but finite, the global requirement (A7) will be localized as

$$\sum_{t' \in p'} \left[\sum_{|t-t'| < \delta t_l} B_{p \ni t}(\mathbf{x}) \right] \approx \sum_{t' \in p'} \left[\sum_{|t-t'| < \delta t_l} B_t(\mathbf{x}) \right], \quad (\text{A8})$$

where $B_{p \ni t}$ is the pixel beam of a pixel that covers \mathbf{x}_t . In the summations over t above (the summations inside the brackets), we have ignored the contribution from $|t - t'| > \delta t_l$ because

the amplitude of $N_{l't}^{-1}$ decays as power law and the central (and maximum) amplitudes of the beams are always unity (i.e. the contribution from $|t - t'| > \delta t_1$ decays as a power law; see eq. [A5]). Therefore, for equation (A8) to hold for the white-noise result (8-3), we require the δt_1 to be much larger than the time required to scan through a pixel, i.e.

$$\frac{\delta t_1}{\delta t} = \frac{1}{2f_1\delta t} \gg \frac{\delta x_p}{\delta x_t}. \quad (\text{A9})$$

To sum up, we know that even if the noise is not white, the white-noise approximation (8-3) is still appropriate as long as

$$f_h \gg \frac{\delta x_t}{\delta t \delta x_p} \gg f_l. \quad (\text{A10})$$

In general, the δx_t and δt are given by experiments, and the δx_p is specified by the pixelization scheme. Therefore, since we normally have $f_h \gg f_l$ in experiments, condition (A10) can be easily satisfied by choosing the right pixel size δx_p . A naive choice will be

$$\delta x_p = \frac{\delta x_t}{\delta t \sqrt{f_h f_l}}, \quad (\text{A11})$$

but in fact one would usually like to choose a pixel size closer to the smallest limit to fully take advantage of the experimental data. In conclusion, one should choose a pixelization scheme whose pixel sizes satisfy condition (A10) (or have an order given by eq. [A11]), so that one can employ the white-noise approximation, which leads to some main results of this paper (see e.g., eqs. [4-10], [8-5], [8-7], [8-10], and [8-12]). If condition (A10) can not be fulfilled (i.e. when the noise spectrum is far from white or $f_h \approx f_l$, which is unlikely to be the case), one can still use the general results (8-2) and (8-8) to calculate the pixel-pixel beam expansion.

REFERENCES

- Bond, J. R., Jaffe, A. H., & Knox L. 1998, Phys. Rev. D, 57, 2117
- Borrill, J. 1999, ‘MADCAP: The Microwave Anisotropy Dataset Computational Analysis Package’ in “Proceedings of the 5th European SGI/Cray MPP Workshop” (see also astro-ph/9911389)
- Crittenden, R. G. & Turok, N. G. 1998, preprint (astro-ph/9806374)
- DeBernardis, P., et al. 2000, Nature, 404, 955
- Ferreira, P. G. & Jaffe, A. H. 2000, MNRAS, 312, 89

Gorski, K. M., Wandelt, B. D., Hansen, F. K., Hivon, E., & Banday, A. J. 1999, preprint
(astro-ph/9905275)

Hanany, S., Jaffe, A. H., & Scannapieco, E. 1998, MNRAS, 299, 653

Hanany, S., et al. 2000, ApJ, accepted

Miller, A., et al. 1999, ApJ, 524, 1

Torbet, E. et al. 1999, ApJ, 521, 79

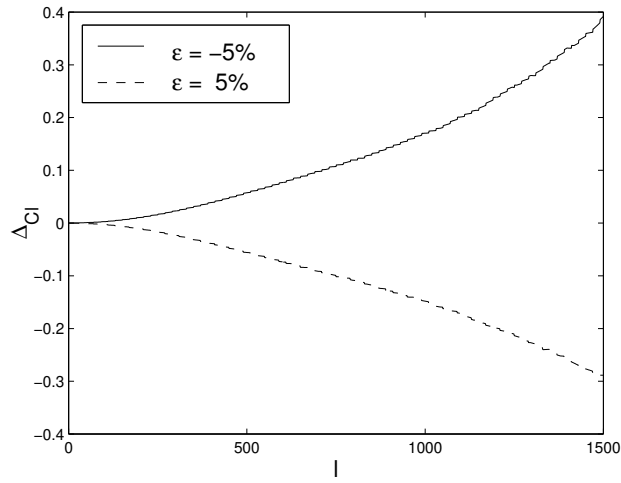


Fig. 13.— Estimated uncertainties, $\Delta_{c_\ell} = dC_\ell/C_\ell$, in the C_ℓ estimates resulting from the beam measurement.